Molecular Therapy
Oncolytics
Original Article

Development of a bicistronic anti-CD19/CD20 CAR construct including abrogation of unexpected nucleic acid sequence deletions

Norris Lam,[1] Richard Finney,[2] Shicheng Yang,[1] Stephanie Choi,[1] Xiaolin Wu,[3] Lauren Cutmore,[1] Jorge Andrade,[4] Lei Huang,[4] Christina Amatya,[1] Margaret Cam,[2] and James N. Kochenderfer[1]

[1]National Institutes of Health, National Cancer Institute, Center for Cancer Research, Surgery Branch, Bethesda, MD, USA; [2]National Institutes of Health, National Cancer Institute, Center for Cancer Research, Office of the Director, Bethesda, MD, USA; [3]Cancer Research Technology Program, Frederick National Laboratory for Cancer Research, Frederick, MD 21701, USA; [4]Kite, A Gilead Company, Santa Monica, CA, USA

To address CD19 loss from lymphoma after anti-CD19 chimeric antigen receptor (CAR) T cell therapy, we designed a bicistronic construct encoding an anti-CD19 CAR and an anti-CD20 CAR. We detected deletions from the expected bicistronic construct sequence in a minority of transcripts by mRNA sequencing. Loss of bicistronic construct transgene DNA was also detected. Deletions of sequence were present at much higher frequencies in transduced T cell mRNA versus gamma-retroviral vector RNA. We concluded that these deletions were caused by intramolecular template switching of the reverse transcriptase enzyme during reverse transcription of gamma-retroviral vector RNA into transgene DNA of transduced T cells. Intramolecular template switching was driven by repeated regions of highly similar nucleic acid sequence within CAR sequences. We optimized the sequence of the bicistronic CAR construct to reduce repeated regions of highly similar sequences. This optimization nearly eliminated sequence deletions. This work shows that repeated regions of highly similar nucleic acid sequence must be avoided in complex CAR constructs. We further optimized the bicistronic construct by lengthening the linker of the anti-CD20 single-chain variable fragment. This modification increased CD20-specific interleukin-2 release and reduced CD20-specific activation-induced cell death. We selected an optimized anti-CD19/CD20 bicistronic construct for clinical development.

INTRODUCTION

Chimeric antigen receptors (CARs) can specifically recognize antigens and activate CAR-expressing T cells.[1–4] Infusions of anti-CD19 CAR T cells have caused prolonged complete remissions of advanced B cell malignancies in many patients[5–13]; however, many aspects of CAR T cell therapies are in need of improvement.[6–9,11,14]

CD19 expression loss is an important mechanism for failure of anti-CD19 CAR T cell therapy. Loss of CD19 expression has been detected in acute lymphoid leukemia[15] and B cell lymphomas.[16] Some cases of B cell lymphoma lack CD19 expression even before anti-CD19 CAR T cell therapy.[16] Because loss of CD19 expression is a known mechanism of failure of anti-CD19 CAR T cell therapy, we designed bicistronic gamma-retroviral CAR constructs that cause a single T cell to express an anti-CD19 CAR and an anti-CD20 CAR. CD20 is expressed by most B cell malignancies.[17–20]

The life cycle of retroviruses includes reverse transcription.[21,22] The RNA genome of retroviruses is reverse transcribed into DNA that makes up the provirus that is integrated into the host cell genome.[21] The reverse transcriptase enzyme that conducts reverse transcription can undergo template switching in which the enzyme switches from one RNA strand to another.[21,23] When the RNA genome of a retrovirus contains repeated regions of highly similar sequence, deletions of sequence from the RNA can occur by a process called intramolecular template switching.[21–24] Intramolecular template switching can occur when two regions of highly similar sequence on the same RNA molecule come into close proximity at the point where reverse transcription is occurring.[21,23–25] This can cause reverse transcriptase to skip part of the RNA sequence, which causes deletion of the sequence.[21,23,24] Because more complex CAR constructs such as bicistronic constructs often have repeated structural components, repeated highly similar nucleic acid sequences can occur in these constructs, so there is a risk for deletion events during reverse transcription of CAR retroviral vector RNA into transgene DNA. We have identified CAR sequence deletions that were likely driven by repeated regions of highly similar sequence in a bicistronic CAR construct. These deletions likely occurred during reverse transcription in transduced T cells. Such deletions lead to transcription of CAR mRNA other than the desired CAR mRNA, so they could reduce expression of the desired CARs. Also, there is a possibility that such deletions

Received 28 April 2022; accepted 17 July 2023;
https://doi.org/10.1016/j.omto.2023.07.001.

Correspondence: James N. Kochenderfer, National Institutes of Health, National Cancer Institute, Center for Cancer Research, Surgery Branch, 10 Center Drive CRC Room 3-3330, Bethesda, MD 20892, USA.
E-mail: kochendj@mail.nih.gov

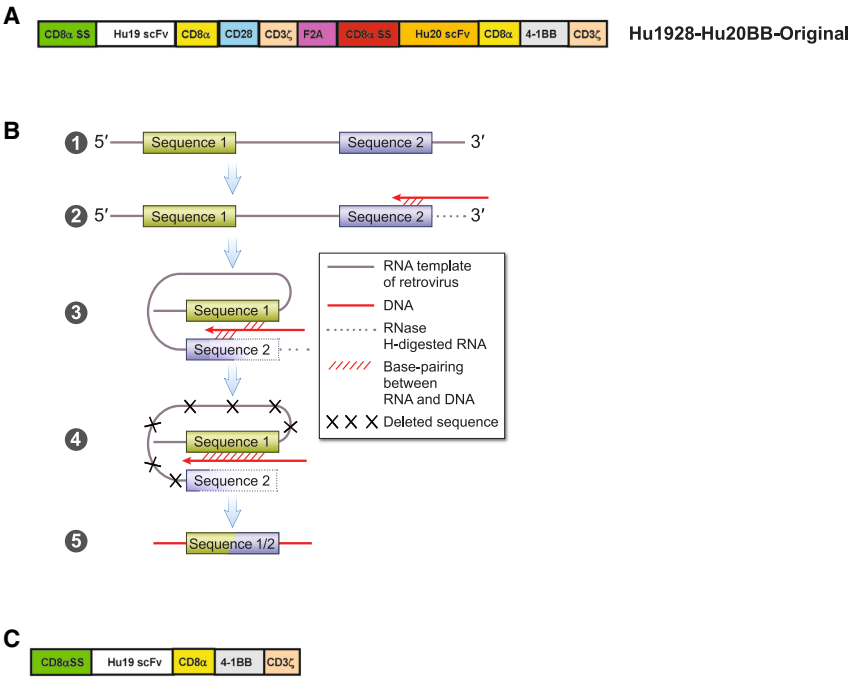

Figure 1. Bicistronic CAR construct Hu1928-Hu20BB-Original and mechanism of deletions of CAR sequence

(A) The first CAR of Hu1928-Hu20BB-Original had a CD8α SS, the Hu19 scFv, a CD8-HTM (CD8α), a CD28 domain, and CD3ζ domain. Next were ribosomal skip and furin domains (F2A). The second CAR had a CD8α SS, the Hu20 scFv, a CD8-HTM, a 4-1BB domain, and a CD3ζ domain. The first CAR of Hu1928-Hu20BB-Original was the anti-CD19 CAR Hu19-CD828Z. The second CAR of Hu1928-Hu20BB-Original was the anti-CD20 CAR Hu20-CD8BBZ. (B) The diagram depicts how intramolecular template switching causes sequence deletions during reverse transcription. Deletions caused by intramolecular template switching could occur in T cells transduced with a retroviral vector encoding a CAR construct. This process is driven by base pairing of nascent DNA to two repeated regions of highly similar sequence in the retroviral genomic RNA. (1) Genomic retroviral RNA with repeated highly similar regions of sequence (sequence 1 and sequence 2). (2) Reverse transcription begins at the 3′ end of the genomic RNA. (3) If two regions of highly similar RNA sequence come into close proximity, simultaneous base pairing can occur between both of the highly similar repeated RNA sequences and the nascent DNA strand. RNase H digests RNA after it has been reverse transcribed. (4) Intramolecular template switching can occur, so reverse transcription continues at the 5′ region of repeated highly similar RNA sequence (sequence 1) instead of the 3′ region of repeated highly similar sequence (sequence 2) where reverse transcription was occurring before the template switch. (5) One copy of the repeated highly similar sequence is deleted from the final DNA transgene, and the sequence between the repeated regions of highly similar sequence is deleted. The remaining copy of highly similar sequence is partially derived from each of the repeated highly similar regions of vector RNA (sequence1/2). Diagram adapted from Delviks et al.[23] (C) A diagram of the aberrant CAR created when sequence between the two CD8-HTM domains of Hu1928-Hu20BB-Original is deleted. The aberrant CAR has a CD8α SS, Hu19 scFv, CD8-HTM, a 4-1BB moiety, and a CD3ζ domain.

could lead to dangerous changes in CAR sequence, such as an undesired new antigen-recognition sequence that could cause the CAR to recognize normal cells. We have developed an optimized bicistronic anti-CD19/CD20 CAR construct to minimize deletion events and to optimize CAR function.

RESULTS

Anti-CD19/CD20 CAR construct

To address CD19-negative B cell lymphoma, we designed a bicistronic CAR construct designated Hu1928-Hu20BB-Original. Hu1928-Hu20BB-Original was designed to allow T cells to simultaneously express two CARs, an anti-CD19 CAR designated Hu19-CD828Z and an anti-CD20 CAR designated Hu20-CD8BBZ (Figure 1A). Both of these CARs have single-chain variable fragment (scFv) binding domains derived from fully human antibodies. Both CARs have hinge and transmembrane domains from CD8α (CD8-HTM) and CD3ζ T cell activation domains. Hu19-CD828Z has a CD28 costimulatory domain, and Hu20-CD8BBZ has a 4-1BB costimulatory domain. Hu1928-Hu20BB-Original is encoded by the MSGV1 gamma-retroviral vector.[26]

Mechanism of sequence deletions

Retroviral gene therapy vectors encoding CARs contain an RNA genome that is reverse transcribed during T cell transduction. Vector RNA can sometimes contain repeated highly similar sequences. During reverse transcription, the nascent DNA strand that is annealed via base pairing to one copy of a repeated vector RNA sequence can simultaneously anneal to an upstream copy of the repeated RNA sequence. This can cause the reverse transcriptase enzyme to undergo intramolecular template switching to the upstream copy of the repeated RNA sequence (Figure 1B).[21,24] Intramolecular template switching can result in deletion of transgene DNA corresponding with one copy of the repeated vector RNA sequence and the sequence between the two regions of repeated vector RNA sequence (Figure 1B).[21,24] Because the integrated transgene is the template for CAR mRNA, intramolecular template switching can lead to deletions of CAR amino acid sequence.

Deletions in Hu1928-Hu20BB-original

Southern blots of DNA from T cells transduced with Hu1928-Hu20BB-Original showed a dominant band of the expected CAR transgene length and no aberrant bands after 21 h of exposure; however, when exposure was extended to 8 days to increase Southern blot sensitivity, single bands of unexpectedly short length, indicating shorter transgene length, became visible in DNA from four donors (Figure S1). This aberrant band was consistent with deletion of part of the transgene sequence.

Table 1. Percentage of mRNA transcripts with deletions starting in each domain of Hu1928-Hu20BB constructs as assessed by SMRT RNA-seq

CAR domain where deletions started	Hu1928-Hu20BB-original	Hu1928-Hu20BB-STD	LONG
Hu19 light chain domain	1.5	0	0
Hu19 heavy chain domain	1.8	0	0.1
First CD8-HTM	18.8	0	0.1
CD28	0	0	0
First CD3ζ	0	0	0
Hu20 light chain domain	0	0	0
Hu20 heavy chain domain	0	0	0
Second CD8-HTM	0.1	0.2	0.2
4-1BB	0	0	0
Second CD3ζ	0	0	0

Cells from 4 donors were transduced with transiently produced MSGV1-Hu1928-Hu20BB-Original vector. Two donors each were transduced with transiently produced MSGV1-Hu1928-Hu20BB-STD or MSGV1-LONG vectors.
mRNA was analyzed by SMRT RNA-seq analysis. Values are the mean percentages of transcripts that had deletions of the expected sequences starting in the listed CAR domains. Only deletions occurring in at least 4 transcripts are included. Only deletions with mRNA sequence 5′ and 3′ to the missing sequence are included. Values less than 0.1% are entered as 0. CD8-HTM means CD8α hinge and transmembrane domain.

Table 2. Percentages of mRNA transcripts with deletions starting in each domain of Hu1928-Hu20BB constructs as assessed by short-read RNA-seq

CAR domain where deletions started	Hu1928-Hu20BB-original	Hu1928-Hu20BB-STD	LONG
Hu19 light chain domain	0.1	0.1	0.1
Hu19 heavy chain domain	0	0	0.1
First CD8-HTM	2.1	0	0
CD28	0	0	0
First CD3ζ	0	0	0
Hu20 light chain domain	0	0.1	0
Hu20 heavy chain domain	0	0.1	0.1
Second CD8-HTM	0	0.3	0.2
4-1BB	0	0	0
Second CD3ζ	0	0.1	0

Cells from four donors were transduced with transiently produced MSGV1-Hu1928-Hu20BB-Original vector. Two donors each were transduced with transiently produced MSGV1-Hu1928-Hu20BB-STD or MSGV1-Hu1928-Hu20BB-LONG vectors.
mRNA from the cells of the donors was analyzed by short-read (Illumina) RNA-seq analysis. Values are the mean percentages of transcripts that had deletions of the expected sequences starting in the listed CAR domains. Only deletions occurring in at least 4 transcripts are included. Only deletions with mRNA sequence 5′ and 3′ to the missing sequence are included. Values less than 0.1% are entered as 0. CD8-HTM means CD8α hinge and transmembrane domain.

To look for Hu1928-Hu20BB-Original sequence deletions, we assessed mRNA from transduced T cells by single-molecule (long-read) real-time mRNA sequencing (SMRT). Deletions of Hu1928-Hu20BB-Original mRNA sequence between regions of repeated highly similar sequence were detected by SMRT. The most common location for deletions to start was the CD8-HTM domain of the first CAR in the construct, Hu19-CD828Z. Most deletions starting in the Hu19-CD828Z CD8-HTM ended in the CD8-HTM region of the second CAR, Hu20-CD8BBZ. Deletion of the nucleic acids between the CD8-HTM domains resulted in an aberrant CAR mRNA transcript with one CD8-HTM sequence containing part of each of the original CD8-HTMs. The CD8-HTM had the amino acid sequence expected in Hu1928-Hu20BB-Original. This CAR also had an Hu19 scFv, a 4-1BB costimulatory domain, and a CD3ζ domain (Figure 1C). Less commonly, deletion events were detected between regions of highly similar sequence shared by the heavy chain domains or the light chain domains of the two CARs in Hu1928-Hu20BB-Original. Both CD3ζ domains in Hu1928-Hu20BB-Original serendipitously had quite different nucleotide sequences. Table 1 summarizes deletions of the expected Hu1928-Hu20BB-Original mRNA sequences. For these experiments, mRNA was obtained from transduced T cells of four donors and assessed by SMRT. Detailed summaries of deletions detected in each region of Hu1928-Hu20BB-Original by SMRT analysis are presented in Figure S2. As a control, we performed SMRT analysis with the same methods used for data in Table 1 on mRNA from T cells expressing the anti-BCMA CAR FHVH33-CD8BBZ[27]; the only deletion in this CAR sequence occurred at a frequency of 0.2% in the CD8-HTM domain.

We confirmed deletions in CAR mRNA transcripts by short-read mRNA sequencing (RNA-seq). Deletion locations determined by short-read RNA-seq were nearly identical to deletion locations determined by SMRT; however, the incidence of deletions detected by short-read RNA-seq was lower than the incidence of deletions detected by SMRT (Table 2). A summary of the short-read RNA-seq analysis for Hu1928-Hu20BB-Original is presented in Figure S3. We detected similar deletions by analyzing the same short-read RNA-seq data with a second data analysis method (Table S1). The amino acid sequences resulting from the two most common deletions determined by the second short-read RNA-seq analysis method are found in Figure S4.

Most deletions had repeated regions of highly similar sequence surrounding the starting and ending points of the deletion. Repeated highly similar sequence segments surrounding the starting and ending points of a deleted region of sequence are consistent with the mechanism of intramolecular template switching occurring during reverse transcription (Figure 1B). The Hu1928-Hu20BB-Original DNA sequences surrounding the starting and ending points of the two most frequent deletions detected in one donor's T cell mRNA by SMRT are indicated in Figure 2. As in mRNA from other donors, the most common starting points for deletions were in the CD8-HTM domain of the first CAR in Hu1928-Hu20BB-Original, Hu19-CD828Z, and the most common ending points of deletions were in the CD8-HTM of the second CAR in the construct, Hu20-CD8BBZ.

Deletions in gamma-retroviral vector RNA

To assess for the possibility of CAR sequence deletions occurring during gamma-retroviral vector production, we assessed RNA from

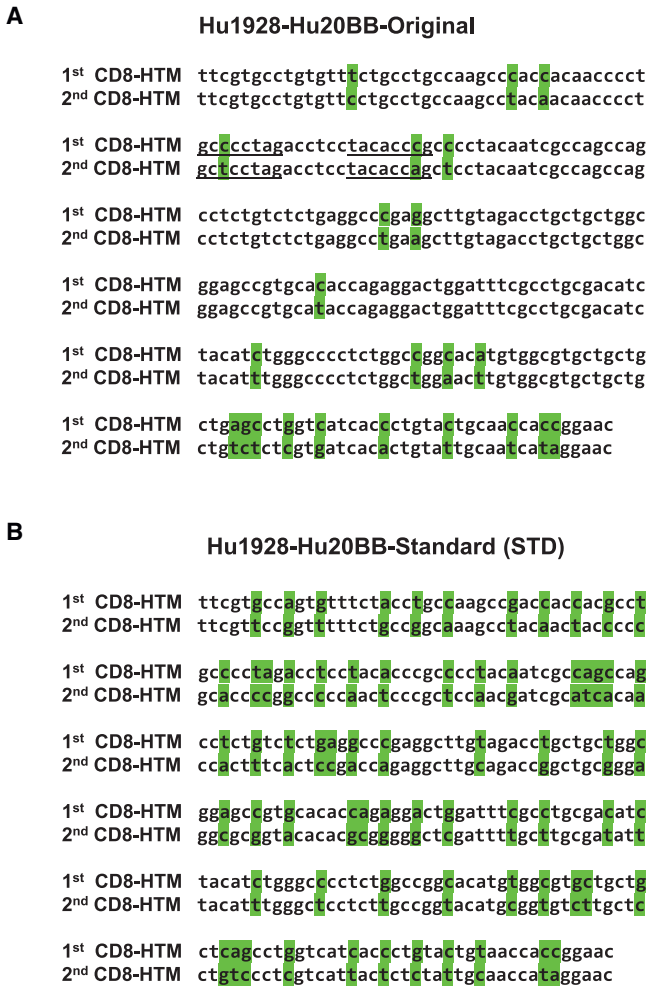

Figure 2. Alignment of the first and second CD8-HTM domains of CAR constructs

(A) DNA sequences of the first and second CD8-HTM domains of Hu1928-Hu20BB-Original are aligned, and nucleotides that are different between the two regions are highlighted in green. The first CD8-HTM is in Hu19-CD828Z, and the second CD8-HTM is in Hu20-CD8BBZ. Only the CD8-HTM sequences are shown without the sequence between the two CD8-HTM domains. Deletions were detected by SMRT in mRNA transcripts from T cells transduced with a gamma-retroviral vector encoding Hu1928-Hu20BB-Original. The two regions of underlined nucleotides in the first CD8-HTM domain indicate the eight nucleotides immediately 5′ to the two most commonly deleted regions of sequence. The nucleotides "tacacccg" were the eight nucleotides immediately 5′ to the start of the most common deletion. The deleted region started with "cccc." The nucleotides "gcccctag" were the eight nucleotides immediately 5′ to the start of the second most common deletion. The deleted region started with "acct." The underlined nucleotides in the second CD8-HTM sequence are the last nucleotides at the 3′ ends of the two most common deletions. (B) DNA sequence of the first and second CD8-HTM domains of Hu1928-Hu20BB-STD are aligned, and nucleotides that are different between the two regions are highlighted in green. Changes were made in the nucleotide sequence of Hu1928-Hu20BB-Original to obtain the sequence of STD. Compared with Hu1928-Hu20BB-Original, STD has fewer regions of highly similar sequence.

MSGV1-Hu1928-Hu20BB-Original gamma-retroviral vector particles by using short-read RNA-seq. We found a low incidence of deletions (Figure S5). For example, the mean incidence of deletions starting in the first CD8-HTM of Hu1928-Hu20BB-Original was 2.1% when transduced T cell mRNA was assessed by short read RNA-seq (Table 2). In contrast, the incidence of gamma-retroviral vector RNA deletions starting in the first CD8-HTM of Hu1928-Hu20BB-Original was only 0.3% when RNA of gamma-retroviral vector particles was studied by short-read RNA-seq. The signal sequence of Hu19-CD828Z had a gamma-retroviral vector RNA deletion with a frequency of 0.1%. No other deletion occurred in the gamma-retroviral vector RNA with a frequency of 0.1% or more. We concluded that most deletions occurred in transduced T cells during reverse transcription.

Deletions of CAR sequence were present in integrated transgene DNA

We wanted to assess the integrated transgene DNA of Hu1928-Hu20BB-Original for sequence deletions. Direct DNA sequencing of the integrated transgene was not feasible because of the low transgene copy number. We used PCR to amplify the integrated transgene for sequencing; however, sequence deletions occurred during PCR reactions. We hypothesized that these deletions were caused by recombination events as previously reported during PCR.[28] To prevent possible recombination events during standard PCR, we designed digital droplet PCR (ddPCR) assays. In ddPCR, the PCR reaction is partitioned into a large number of droplets. Each droplet contains a separate amplification reaction. We set up ddPCR reactions to make it unlikely that any droplet contained more than one DNA template molecule. We designed three PCR reactions for use with Hu1928-Hu20BB-Original. One PCR reaction amplified the Hu19-CD828Z CD8-HTM. A second PCR reaction amplified the Hu20-CD8BBZ CD8-HTM. A third PCR product was generated only when the DNA separating the Hu19-CD828Z CD8-HTM and the Hu20-CD8BBZ CD8-HTM was deleted in transduced T cells before DNA was obtained for ddPCR (Figure S6). With this approach, we detected deletions of DNA between the two CD8-HTM domains of Hu1928-Hu20BB-Original in a mean of 4.6% of transgene DNA copies.

Optimization of CAR sequences to reduce sequence deletions

To address CAR sequence deletions that were likely driven by repeated highly similar nucleic acid sequences in Hu1928-Hu20BB-Original, we optimized the DNA sequence of Hu1928-Hu20BB-Original to reduce repeated highly similar regions of DNA sequence. First, we replaced the CD8α signal sequence of the Hu20-CD8BBZ CAR with the signal sequence of the granulocyte-macrophage colony-stimulating factor receptor α-chain (GM-CSFr) that was used in a previous CAR.[29] Next, we assessed the DNA sequence of Hu1928-Hu20BB-Original for repeated identical DNA sequences of eight or more continuous nucleotides. Usually, one repeat of highly similar sequence was in Hu19-CD828Z, and the second repeat of highly similar sequence was in Hu20-CD8BBZ; for example, repeated regions of identical nucleic acid sequence were found in the CD8-HTM domains of both CARs. We used the DNA sequence of

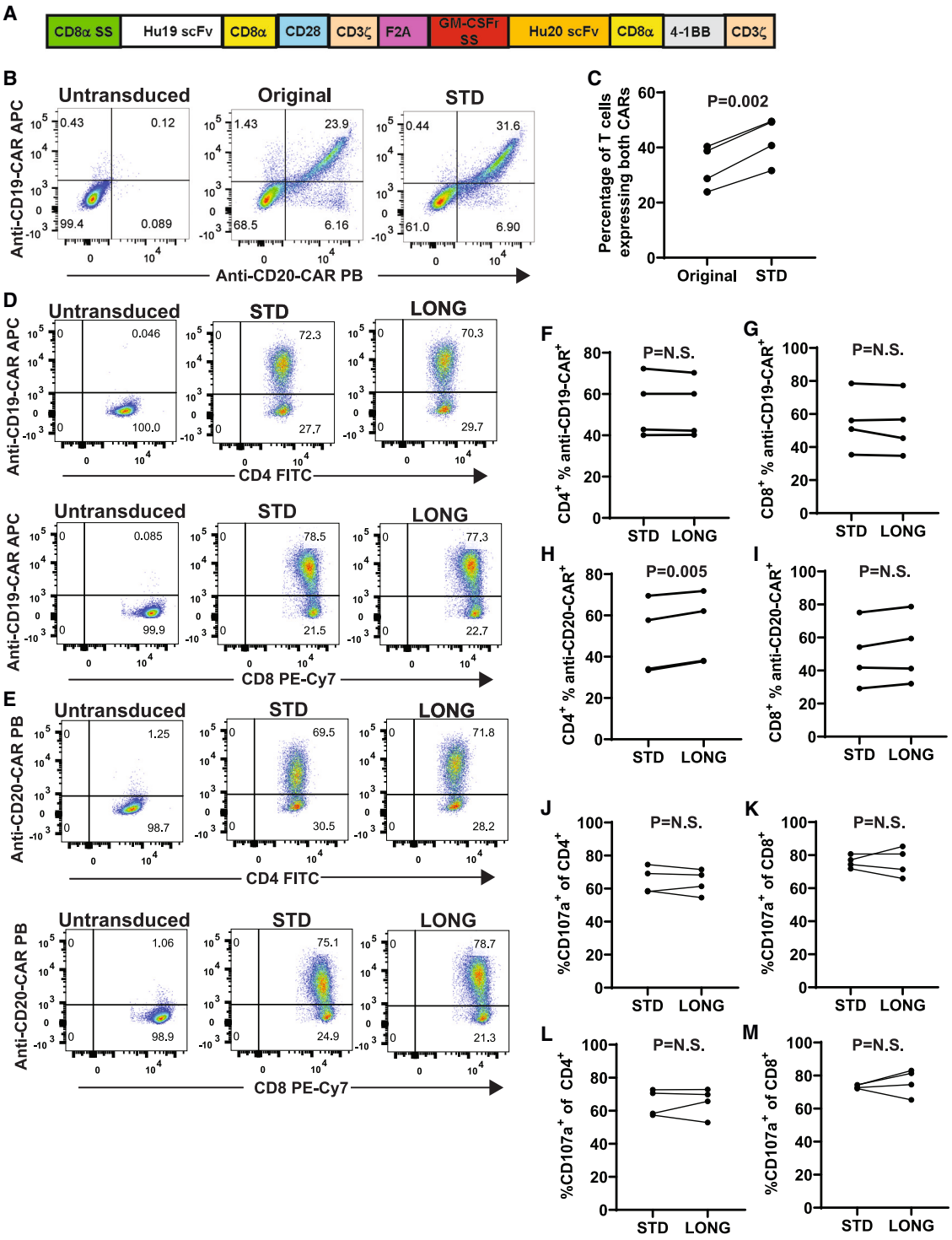

Figure 3. Expression of two functional CARs by bicistronic CAR constructs

(A) A diagram of the STD construct is shown. The first CAR of STD had a CD8α SS (CD8α SS), the Hu19 scFv, CD8-HTM (CD8α), a CD28 domain, and a CD3ζ domain. Next, were F2A and furin sequences (F2A). The second CAR had a GM-CSF-receptor-α SS (GM-CSFr SS), the Hu20 scFv, CD8-HTM, a 4-1BB domain, and a CD3ζ domain. (B) Human PBMC were stimulated with anti-CD3 in IL-2-containing media. Two days later, transductions were conducted. Five days after transductions, flow cytometry was conducted to assess CAR expression. Plots gated on live $CD3^+$ lymphocytes show combined expression of anti-CD19 CARs and anti-CD20 CARs on T cells transduced with

(legend continued on next page)

Hu1928-Hu20BB-Original as a template for designing a new DNA sequence that lacked repeated regions of identical sequence while maintaining the same amino acid sequence. Redundancy of the nucleotide codes for most amino acids allows the same amino acids to be encoded by multiple nucleotide sequences. We made the most changes to the CD8-HTM domains (Figure 2). Changes in DNA sequence were made in an iterative manner, and CAR expression testing was conducted for each new version of the construct. For expression testing, T cells were transduced with gamma-retroviral vectors encoding each new version, and CAR expression was assessed by flow cytometry. This was done because DNA sequence changes might have caused a decrease in CAR expression. Fortunately, CAR expression increased with the DNA changes. The seventh version was designated Hu1928-Hu20BB-Standard (STD) (Figure 3A). Compared with Hu1928-Hu20BB-Original, STD had both higher CAR expression and greatly decreased repeated regions of highly similar DNA sequence. CAR expression on human T cells was higher with the STD construct compared with Hu1928-Hu20BB-Original when T cells were assessed for CAR expression (Figures 3B and 3C).

Increased Hu20 scFv linker length

We hypothesized that altering the linker of the Hu20 scFv might affect CAR function. The STD construct was further modified by lengthening the linker of the scFv of the Hu20-CD8BBZ CAR. The linker of the scFv of Hu20-CD8BBZ consisted of three repeats of glycine-glycine-glycine-glycine-serine (G-G-G-G-S). We added one additional repeat to this linker to make a linker with four G-G-G-G-S repeats; the anti-CD20 CAR with the longer linker was called Hu20-CD8BBZ-Long (Hu20-CD8BBZ-L). The overall anti-CD19/CD20 CAR construct with the Hu20-CD8BBZ-L CAR and reduced regions of highly similar sequence was designated Hu1928-Hu20BB-Long (LONG). Except for the longer scFv linker in the Hu20-CD8BBZ-L CAR of LONG, the LONG construct had the same sequence as the STD construct.

Deletion frequencies of optimized bicistronic CAR constructs

We assessed STD and LONG for sequence deletions similar to those previously detected in Hu1928-Hu20BB-Original. We transduced T cells with gamma-retroviral vectors encoding these constructs and performed RNA-seq on mRNA from the T cells. Sequence deletions in the optimized constructs STD and LONG were nearly eliminated as assessed by either SMRT or short-read RNA-seq (Tables 1 and 2; Figures S7 and S8).

In vitro expression and function of STD versus LONG

We conducted a series of *in vitro* experiments to compare T cells expressing the STD construct with T cells expressing the LONG construct. Expression of the Hu19-CD828Z CAR was detected on T cells transduced with either STD or LONG by flow cytometry with an antibody specific for this CAR (Figure 3D). The same T cells were assessed for expression of the anti-CD20 CARs Hu20-CD8BBZ in STD or Hu20-CD8BBZ-L in LONG. The anti-CD20 CARs contained the Hu20 scFv. Expression was assessed by flow cytometry with an antibody specific for the Hu20 scFv (Figure 3E). For both $CD4^+$ and $CD8^+$ T cells, there was not a statistically significant difference in Hu19-CD828Z expression when STD and LONG were compared (Figures 3F and 3G). In the same T cells assessed for Hu19-CD828Z expression, we compared expression of Hu20-containing CARs. There was not a statistically significant difference in expression for $CD8^+$ T cells, but there was a statistically higher level of Hu20-containing CAR expression with LONG versus STD in $CD4^+$ T cells (Figures 3H and 3I). One possible contributing factor to the difference in expression of Hu20-CD8BBZ versus Hu20-CD8BBZ-L in $CD4^+$ T cells was that the longer linker in the Hu20 scFv of Hu20-CD8BBZ-L might affect binding of the anti-CD20-CAR antibody used to measure expression of the Hu20-containing CARs.

The ability to produce CAR^+ T cells was not affected by use of STD versus LONG. We stimulated T cells with an anti-CD3 antibody, and transduced 2×10^6 cells on day 2 of culture. On day 7 of culture, the median numbers of CAR^+ cells obtained were 14.96×10^6 (range, $23.58–6.72 \times 10^6$) for STD and 13.25×10^6 (range, $27.67–4.81 \times 10^6$) for LONG ($p = 0.867$ by paired t test; $n = 4$).

Next, we assessed the function of T cells expressing STD versus LONG by performing degranulation assays. Degranulation assays were performed by measuring CD107a expression after culturing CAR T cells with target cells. There were no statistically significant differences in degranulation of T cells expressing STD versus LONG when target cells were st486 cells, which express both CD19 and CD20 (Figures 3J and 3K). Because the only difference between STD and LONG is the length of the Hu20 scFv linker, we also assessed degranulation with CD19-negative, $CD20^+$ st486-CD19neg target cells. There were no statistically significant differences in degranulation when st486-CD19neg target cells were used for either $CD4^+$ (Figure 3L) or $CD8^+$ (Figure 3M) T cells.

Hu1928-Hu20BB-Original (Original) or STD. (C) Four experiments with cells from different donors were conducted as in (B). Statistical comparison was by two-tailed, paired t test. (D) Anti-CD19-CAR and (E) anti-CD20-CAR antibody staining was assessed on $CD4^+$ and $CD8^+$ T cells transduced with STD or LONG as described in (B). Untransduced T cells are also shown. Plots are gated on live $CD3^+$ lymphocytes. Percentages of (F) $CD4^+$ and (G) $CD8^+$ T cells that stained with the anti-CD19-CAR antibody were compared. T cells were transduced and flow cytometry was performed as in (D). Percentages of (H) $CD4^+$ and (I) $CD8^+$ T cells that stained with the anti-CD20-CAR antibody were compared. T cells were transduced and flow cytometry was performed as in (E). (J) $CD3^+CD4^+$ and (K) $CD3^+CD8^+$ T cells expressing STD or LONG were cultured for 4 h with st486 cells in the presence of an antibody against CD107a. Cells were assessed by flow cytometry for CD107a expression on live T cells. (L) $CD3^+CD4^+$ and (M) $CD3^+CD8^+$ T cells were assessed for CD107a expression as in (J) and (K), except st486-CD19neg target cells were used. For (F–M), statistical comparisons were two-tailed paired t tests; $n = 4$ different donors. N.S., not statistically significant. Throughout the figure, dots connected by lines represent results of the same patient's cells transduced with the indicated constructs.

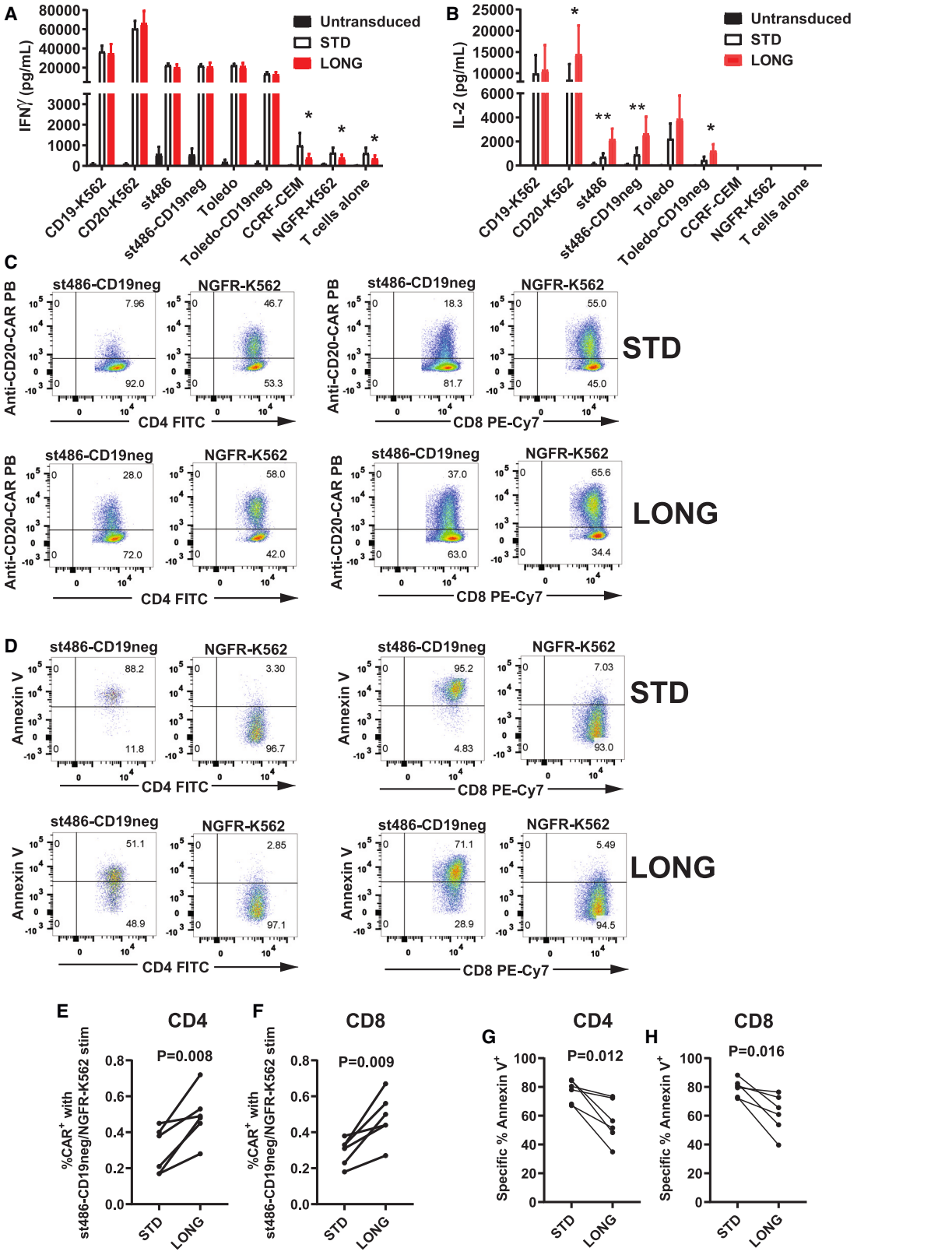

(legend on next page)

Increased CD20-specific IL-2 release by T cells expressing LONG versus STD

Seven days after transduction, T cells transduced with either STD or LONG were cultured overnight with the target cells indicated in Figure 4A, and an interferon-gamma (IFN-γ) ELISA was performed on culture supernatants. The only statistically significant differences were increased IFN-γ release for STD versus LONG when T cells were cultured alone or with control target cells lacking both CD19 and CD20 expression. We compared interleukin-2 (IL-2) production by T cells expressing STD versus LONG by ELISA. We found that IL-2 production was statistically higher for LONG versus STD when $CD20^+$, CD19-negative target cells CD20-K562, st486-CD19neg, and Toledo-CD19neg were used. IL-2 production was also higher for LONG versus STD when st486 target cells were used. st486 cells express high levels of CD20 and low levels of CD19. This difference in IL-2 production only with target cells that expressed high levels of CD20 and low or absent levels of CD19 is notable because the only difference in STD and LONG is the length of the scFv linker of the Hu20-containing CARs that target CD20. We did not detect a statistically significant difference in proliferation when T cells expressing either STD or LONG were compared (Figure S9).

Reduced activation-induced cell death in T cells expressing LONG versus STD

We conducted experiments to determine if the longer scFv linker in LONG affected CAR T cell susceptibility to activation-induced cell death (AICD) when CAR T cells were stimulated with $CD20^+$ target cells. T cells expressing STD or LONG were cultured for 4 h with st486-CD19neg target cells or NGFR-K562 target cells. The T cells were then assessed for Hu20-CAR expression by flow cytometry with the anti-CD20-CAR antibody. Hu20-CAR is used to refer to both Hu20-CD8BBZ of STD and Hu20-CD8BBZ-L of LONG. In comparison with CAR T cells cultured with CD20-negative NGFR-K562, decreased levels of Hu20-CAR^+ T cells were present when CAR T cells were cultured with $CD20^+$ st486-CD19neg cells (Figure 4C). Cells from six donors were stimulated with st486-CD19neg or NGFR-K562 cells. For both $CD4^+$ T cells (Figure 4E) and $CD8^+$ T cells (Figure 4F), reduction in percent Hu20-CAR^+ T cells was statistically greater for STD versus LONG. Loss of Hu20-CAR^+ cells could be caused by two different processes. First, cells could die and disappear from cultures before the end of the assay, so the cells would not be detected by flow cytometry. Second, CAR expression downregulation could occur. Figure S10 shows the percentages of T cells that were Hu19-CD828Z CAR^+ in the experiments reported in Figures 4E and 4F. After st486-CD19neg stimulation, the magnitude of the decrease in Hu20-CAR^+ cells was much greater than the magnitude of the decrease in Hu19-CD828Z CAR^+ cells. In addition, there was not a statistically significant difference in Hu19-CD828Z loss when STD and LONG were compared (Figures 4E, 4F, and S10). These findings indicate that the Hu20-CAR^+ cell loss was mostly caused by CD20-dependent CAR downregulation. If CAR^+ cell loss was caused by cell death, the magnitude of Hu19-CD828Z-expressing cell loss should have been similar to the magnitude of Hu20-CAR^+ cell loss because the same T cells usually express both Hu19-CD828Z and Hu20-CARs (Figure 3B).

We assessed the same cells that were evaluated for CAR^+ cell loss for apoptosis by annexin V staining. We focused on Hu20-CAR-expressing cells as determined by flow cytometry. We found that substantial apoptosis occurred with both STD and LONG T cells (Figure 4D). Annexin V was statistically higher for STD versus LONG for $CD4^+$ and $CD8^+$ T cells (Figures 4G and 4H).

In vitro cytotoxicity and *in vivo* tumor elimination by T cells expressing STD or LONG

T cells expressing either STD or LONG efficiently killed target cells *in vitro*, and there was minimal difference in cytotoxicity when STD and LONG were compared (Figure 5A). We compared *in vivo* anti-tumor activity of human T cells expressing either STD or LONG. We established tumors of $CD19^+$, $CD20^+$ st486 cells in immunocompromised nod-scid common γ-chain knockout mice (NSG, NOD.Cg-*Prkdc*^{scid} *Il2rg*^{tm1Wjl}/SzJ). When we treated tumors with 1×10^6 CAR^+ T cells/mouse, tumor elimination and survival were not different for T cells expressing STD versus LONG, and T cells expressing either STD or LONG effectively eliminated tumors (Figures 5B and 5C). We assessed T cells expressing either STD or LONG for the ability to eradicate tumors of CD19-negative, $CD20^+$ st486-CD19neg cells. T cells expressing either STD or LONG could eliminate tumors in some, but not all, mice at a dose of 0.5×10^6

Figure 4. Lengthening the linker of the Hu20 scFv affects function of CAR T cells

(A) T cells transduced with the indicated CAR constructs or left untransduced were cultured overnight with target cells. IFN-γ ELISA was performed on culture supernatants; n = 4 different donors. CD19-K562 target cells expressed CD19. CD20-K562, st486-CD19neg, and Toledo-CD19neg expressed CD20. st486 and Toledo expressed CD19 and CD20. CCRF-CEM and NGFR-K562 were CD19 and CD20 negative. (B) Supernatants from the same CAR T cell plus target cell cultures in A were assessed by ELISA for IL-2; n = 5 donors except n = 4 for Toledo and Toledo-CD19neg. For (A and B), statistics were two-tailed, ratio paired t tests; *$p < 0.05$, **$p < 0.001$. For (A and B), cytokine values were normalized for CAR expression by dividing cytokine values by the fraction of T cells expressing both CARs in the constructs. (C) T cells expressing either STD or LONG were cultured for 4 h with either st486-CD19neg or NGFR-K562 target cells. Cells were stained with the anti-CD20-CAR antibody and analyzed by flow cytometry to assess CAR expression. Plots are gated on $CD4^+$ or $CD8^+$ live (7-aad-negative), $CD3^+$ lymphocytes. (D) Annexin V staining of the same cells as (C). Plots are gated on live anti-CD20-CAR^+CD4^+ or anti-CD20-CAR^+CD8^+ T cells. (E) $CD4^+$ T cells were analyzed as shown in (C). Antigen-specific CAR expression decrease of Hu20-CARs was quantified as the percent anti-CD20-CAR^+ cells with st486-CD19neg stimulation divided by the percent anti-CD20-CAR^+ cells with NGFR-K562 stimulation (%CAR^+ with st486-CD19neg/NGFR-K562 stim). (F) $CD8^+$ T cells from the same cultures as in (E) were analyzed as in (E). (G) Specific %annexin V^+ cells are shown for the same anti-CD20-CAR^+CD4^+ T cells in (E). (H) Specific %annexin V^+ cells are shown for the same anti-CD20-CAR^+CD8^+ T cells in (F). For (G and H), specific %annexin V^+ was calculated as %annexin V^+ CAR^+ T cells with st486-CD19neg stimulation minus the %annexin V^+ CAR^+ T cells with NGFR-K562 stimulation. For (E–H), n = 6 different donors; statistics are two-tailed paired t tests. Dots connected by lines represent results of the same patient's cells transduced with indicated constructs. $p < 0.05$ was considered statistically significant.

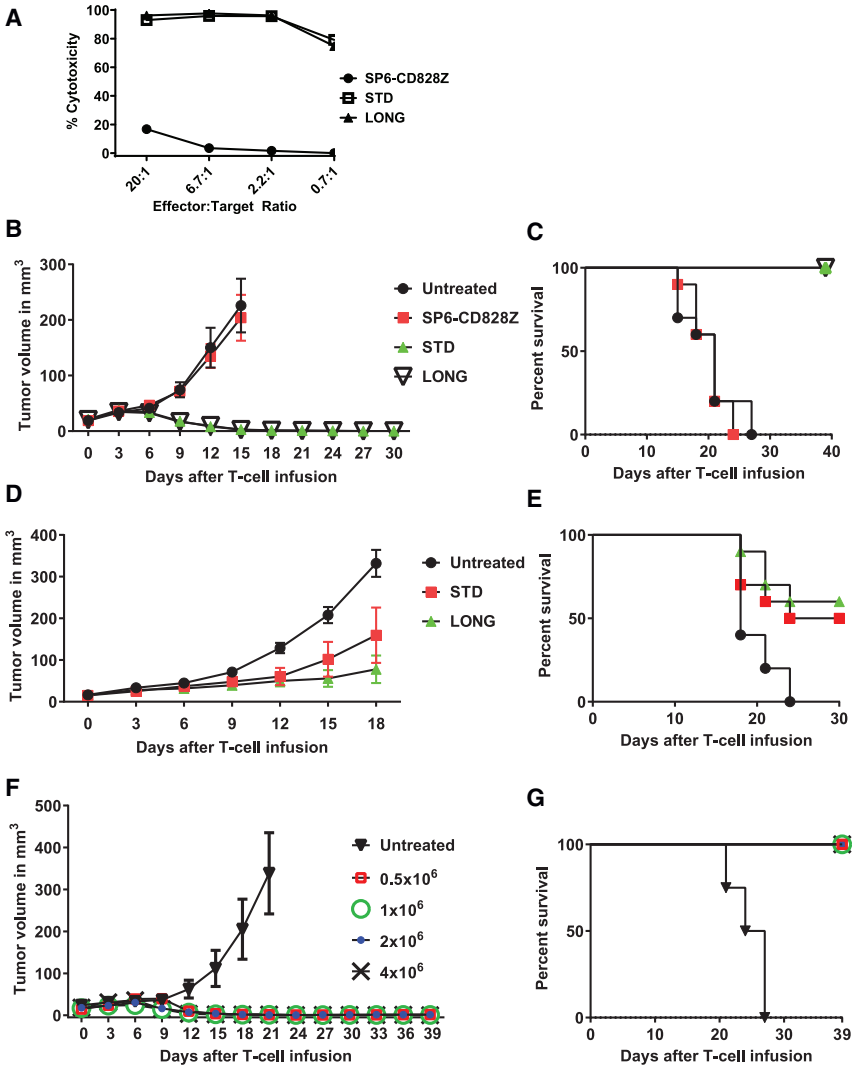

Figure 5. *In vitro* cytotoxicity and xenograft tumor eradication by STD and LONG

(A) Cytotoxicity of T cells expressing STD, LONG, or the negative-control CAR SP6-CD828Z was assessed in a 4-h cytotoxicity assay against Toledo target cells. This is one of two experiments with similar results. (B) Four million st486 cells were injected intradermally into NSG mice. Six days later, when palpable tumors were present, mice were injected intravenously with a single infusion of 1×10^6 CAR^+ T cells or left untreated. Ten mice from two experiments of five mice each are in each group. Each experiment used T cells from a different human donor. In all experiments in this figure, tumor sizes are mean tumor volume ± SEM, and tumor size curves stop when the first mouse of any group was sacrificed or the experiment ended. (C) Kaplan-Meier plots of survival of the same mice as in (B) are shown. Survival was longer when the STD or LONG groups were compared with SP6-CD828Z or untreated ($p < 0.0001$ for all comparisons). There was no difference in survival between STD and LONG. Survival comparison was by log-rank test for this entire figure. $p < 0.05$ was considered statistically significant for this entire figure. (D) Four million st486-CD19neg cells were injected intradermally into NSG mice. Six days later, when palpable tumors were present, mice were left untreated or injected intravenously with a single infusion of 0.5×10^6 CAR^+ T cells per mouse. There were 10 mice per group. Each group included five mice from each of two experiments with cells from a different human donor. (E) Kaplan-Meier plots of survival of the same mice as (D). Survival was longer for STD and LONG compared with Untreated; $p = 0.015$ for STD versus untreated; $p = 0.002$ for LONG versus untreated. There was not a statistically significant difference in survival between STD and LONG. (F) Tumors of st486-CD19neg tumors were established in mice as in (D). Mice were treated with the indicated doses of LONG T cells; n = 4 per group. (G) Survival of mice in (F). All doses of LONG T cells caused statistically significant increases in survival when compared with untreated ($p = 0.009$).

CAR^+ T cells/mouse. (Figure 5D). Treatment with 0.5×10^6 CAR^+ STD or LONG T cells increased survival when compared with untreated mice (Figure 5E). In a different experiment, LONG T cells eradicated st486-CD19neg tumors at CAR^+ T cell doses of 0.5×10^6 CAR^+ T cells per mouse or higher (Figures 5F and 5G).

Expression and function of T cells expressing LONG or its constituent CARs

Because T cells expressing LONG had higher CD20-specific IL-2 production and lower AICD when compared with T cells expressing STD *in vitro*, we focused further experiments on LONG. T cells transduced with LONG expressed both Hu19-CD828Z and Hu20-CD8BBZ-L (Figure 6A). Cytokine release by LONG was antigen-specific (Figure 6B). IFN-γ release was similar for LONG and its constituent CARs. IFN-γ release was not statistically different when T cells expressing either Hu19-CD828Z or LONG were cultured with CD19-K562 targets. IFN-γ release was not statistically different when T cells expressing either Hu20-CD8BBZ-L or LONG were cultured with CD20-K562, st486, or st486-CD19neg. Compared with Hu19-CD828Z and LONG T cells, Hu20-CD8BBZ-L T cells had higher levels of IFN-γ release when cultured alone or with target cells lacking expression of both CD19 and CD20. Antigen-independent function of CARs containing a 4-1BB domain has been shown previously.[30,31] We performed ELISAs to measure IL-2 release from the same cultures that were assessed for IFN-γ release. As with IFN-γ, there were no statistically significant differences in IL-2 release in response to target cells expressing the appropriate antigen when IL-2 release by LONG was compared with IL-2 release by its constituent CARs (Figure S11).

We transduced T cells from the same patients with vectors encoding LONG or Hu19-CD828Z alone or Hu20-CD8BBZ-L alone. When T cells were transduced with LONG or vectors encoding single CARs, similar percentages of T cells expressed the CARs for all conditions except that Hu19-CD828Z expression on $CD8^+$ T cells was

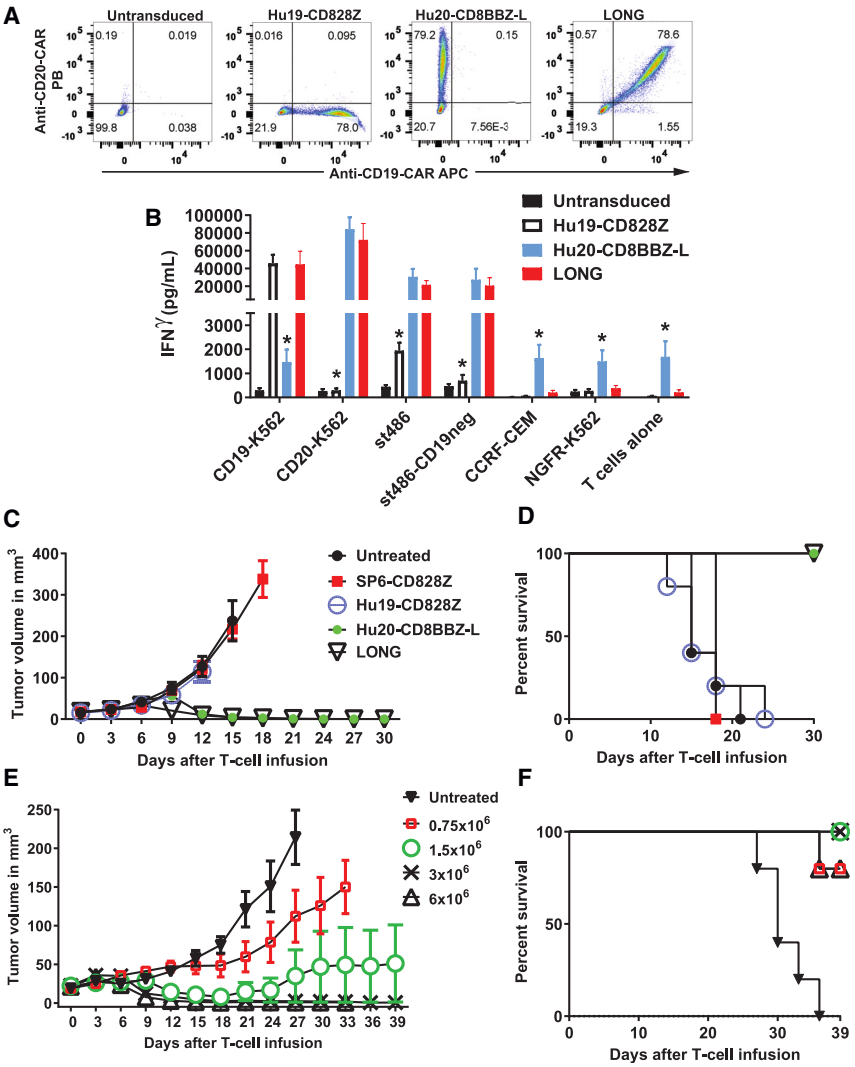

Figure 6. Antigen-specific CAR T cell function

(A) CAR expression on T cells transduced with the indicated constructs was assessed by flow cytometry five days after transduction. Hu19-CD828Z was stained by the anti-CD19-CAR antibody. Hu20-CD8BBZ-L was stained by the anti-CD20-CAR antibody. Plots are gated on live $CD3^+$ cells. Similar results were obtained with nine donors. (B) With $CD19^+$, CD20-negative CD19-K562 target cells, IFN-γ production was statistically lower for Hu20-CD8BBZ-L T cells compared with Hu19-CD828Z T cells and LONG T cells. IFN-γ production was statistically lower with T cells expressing Hu19-CD828Z than T cells expressing Hu20-CD8BBZ-L or LONG when T cells were stimulated with these $CD20^+$, CD19-negative/dim target cells: CD20-K562, st486-CD19neg, and st486. There was not a statistically significant difference in IFN-γ production when Hu19-CD828Z or LONG were cultured with CD19-K562. There was also not a statistically significant difference in IFN-γ production when Hu20-CD8BBZ-L or LONG were cultured with either CD20-K562, st486, or st486-CD19neg. Compared with T cells expressing the other CAR constructs, Hu20-CD8BBZ-L T cells had higher antigen-independent IFN-γ release against negative-control target cells NGFR-K562 and CCRF-CEM. Asterisks indicate CAR types with IFN-γ release that was statistically different at the $p < 0.01$ level when compared with the IFN-γ release of the other two CAR types. Comparison was by two-tailed, ratio paired t test. $p < 0.05$ was considered statistically significant. There was no correction for multiple comparisons. Bars represent mean + SEM; n = 5 donors. Values are pg/mL of IFN-γ normalized for CAR expression. (C) NSG mice were injected with $CD20^+$, CD19-negative CD20-MM.1S cells. Seven days later, when palpable tumors were present, mice were left untreated or received intravenous injections of 3×10^6 CAR^+ human T cells of the indicated types. Values are mean tumor volume ± SEM; n = 5 mice per group. (D) Kaplan-Meier plots of the same mice as (C). By log rank test, survival was longer for both Hu20-CD8BBZ-L and LONG versus each of the other three groups. $p < 0.003$ for all comparisons. (E) NSG mice were injected with NALM6 cells. When palpable tumors were present 6 days later, mice received the indicated number of LONG CAR^+ T cells or were untreated. Values are mean tumor volume ± SEM; n = 5 mice per group. (F) Kaplan-Meier plots of mice from (E). Survival of all LONG groups was longer than survival of untreated mice. $p < 0.005$ by log rank test for all comparisons.

statistically lower on $CD8^+$ T cells transduced with a vector encoding LONG versus $CD8^+$ T cells transduced with a vector encoding Hu19-CD828Z alone (Figures S12A–S12D). The median fluorescence intensity (MFI) of CAR expression was statistically higher when T cells were transduced with vectors encoding either Hu19-CD828Z alone or Hu20-CD8BBZ-L alone versus a vector encoding LONG (Figures S12E–S12H).

We compared antigen-specific degranulation of T cells transduced with LONG or Hu20-CD8BBZ-L alone. For both $CD4^+$ and $CD8^+$ T cells, specific degranulation in response to $CD20^+$ target cells was higher for T cells transduced with LONG versus T cells transduced with Hu20-CD8BBZ-L alone (Figures S13 and S14). A contributing factor for higher levels of CD20-specific degranulation of T cells expressing LONG versus Hu20-CD8BBZ-L alone was the higher level of antigen-independent degranulation by T cells expressing Hu20-CD8BBZ-L alone. This was because CD20-specific degranulation was calculated by subtracting the percentage of T cells degranulating after stimulation with CD20-negative NGFR-K562 cells from the percentage of T cells degranulating after stimulation with $CD20^+$ st486-CD19neg cells. Compared with T cells expressing LONG, T cells expressing Hu20-CD8BBZ-L had higher levels of degranulation after stimulation with NGFR-K562 cells. We established that T cells expressing LONG do not unexpectedly recognize a variety of cell lines and primary cells lacking expression of both CD19 and CD20 (Table S2).

Eradication of CD19-negative tumors by LONG T cells

To further demonstrate that LONG T cells could eradicate CD19-negative tumors, we established tumors of $CD20^+$, CD19-negative

CD20-MM.1S cells in NSG mice, and we treated the mice by injecting T cells expressing LONG, Hu19-CD828Z, or Hu20-CD8BBZ-L. T cells expressing either LONG or Hu20-CD8BBZ-L eradicated tumors, but T cells expressing Hu19-CD828Z had no anti-tumor effect (Figures 6C and 6D). We established tumors of $CD19^+$, $CD20^+$ NALM6 cells in NSG mice and treated the mice with increasing doses of LONG T cells. Tumors were reduced in a dose-dependent manner (Figures 6E and 6F). To assess anti-tumor activity of T cells expressing a bicistronic construct with two CARs containing CD28 costimulatory domains, we designed a CAR construct identical to LONG except the 4-1BB costimulatory domain of the anti-CD20 CAR was replaced with a CD28 costimulatory domain. This CAR was called Hu1928-Hu2028-Long. There were no statistically significant differences in tumor sizes or survival when T cells expressing Hu1928-Hu2028-Long were compared with T cells expressing LONG (Figure S15).

DISCUSSION

To address CD19 loss as a resistance mechanism against anti-CD19 CAR T-cell therapy, we developed an optimized bicistronic CAR construct that included an anti-CD19 CAR and an anti-CD20 CAR. Anti-CD19 CAR T cells have proven efficacy against a variety of B cell malignancies.[8,9,11,13,32] Adding a CAR targeting a second antigen to address CD19 loss is a rational next step because of the proven loss of CD19 from malignant cells after anti-CD19 CAR T-cell treatment.[16] CD20 is a promising second antigen to target, since CD20 is highly expressed on large B cell lymphomas[17,33] and other types of B cell lymphomas.[18,33] CD20 is also expressed on chronic lymphocytic leukemia and some cases of acute lymphoid leukemia.[17,19,20,33,34]

To simultaneously target two antigens by one CAR T cell, two approaches can be used. Tandem CARs consist of one CAR molecule with tandem antigen-binding domains targeting two different antigens; tandem CARs have been tested in multiple clinical trials.[35–39] Tandem CARs include a series of antibody heavy-chain and light-chain variable domains.[37,39] In contrast, bicistronic CAR constructs encode two separate CAR molecules.[35,40] We chose to use the bicistronic approach in our work because we were concerned about possible unexpected effects on antigen recognition with the tandem approach. We had this concern because tandem CARs have a series of variable domains targeting different antigens, and these variable domains are spatially close to each other. Although *in vitro* tests can be performed to assess the specificity of tandem CARs, the slight chance of unexpected *in vivo* reactivity because the proximity of variable domains targeting different antigens cannot be totally ruled out.

Targeting more than one antigen requires CAR constructs that are larger and more complex than typical CARs targeting only one antigen. Tandem CARs targeting more than one antigen have repeated antibody variable domains.[35–39] Bicistronic CAR constructs encode two CARs, so there are two copies of most CAR components (Figure 1A).[35,40] Repeated components might be encoded by similar nucleic acid sequences. We found that deletions of the expected CAR sequence occurred with Hu1928-Hu20BB-Original. These deletions occurred between two regions with highly similar nucleic acid sequences. We confirmed that these deletions were present in CAR mRNA from transduced T cells by SMRT and short-read RNA-seq. We also demonstrated that the deletions were present at the transgene level in the DNA of transduced T cells. The deletion events likely occurred during reverse transcription because the frequency of deletions was much lower in RNA from the gamma-retroviral vector particles used to transduce T cells compared with the frequency of deletions in mRNA from transduced T cells. The most common mechanism of deletions occurring during reverse transcription is intramolecular template switching by the reverse transcriptase enzyme.[21,23,24] Intramolecular template switching has been previously studied in natural retroviruses; the template switching is driven by repeated highly similar regions of nucleic acid sequence.[21,23–25] The frequency of deletions was highest between the two CD8-HTM domains. This was likely because, compared with any other two CAR domains, the two CD8-HTM domains shared more identical regions of nucleic acid sequence. Deletions such as those observed with the gamma-retroviral vector used in this work have been observed with human immunodeficiency virus, which is a lentivirus[21]; therefore, we expect that similar deletions could occur with lentiviral CAR vectors. We optimized the sequence of Hu1928-Hu20BB-Original to eliminate extended regions of highly similar nucleic acid sequence. This greatly reduced the frequency of deletions (Tables 1 and 2; Figure 2). After sequence optimization to reduce deletions, expression of the CARs encoded by bicistronic anti-CD19/CD20 CAR constructs improved (Figure 3A). Our work shows that repeated highly similar regions of CAR nucleic acid sequence should be avoided to reduce unexpected deletions of CAR sequence and to increase expression of the desired CAR sequence. This finding is especially important as more complex CAR constructs are being developed.[35–40]

The deletion frequencies that were detected with SMRT versus short-read RNA-seq were different (Tables 1 and 2). This could be caused by both technical differences in the sequencing methods and by differences in how the sequencing results were analyzed. A possibly important factor is that one of the first steps of performing SMRT was an *in vitro* reverse transcription step. Deletions due to intramolecular template switching might have occurred during this reverse transcription step, or deletions might have occurred during the subsequent PCR step of the SMRT process. The short-read RNA-seq method is quite different. During short-read RNA-seq, the mRNA sample was fragmented into short pieces of approximately 150 base pairs before reverse transcription. This fragmentation made *in vitro* intramolecular template switching highly unlikely when repeated regions of highly similar sequence were separated by more than approximately 150 base pairs. The high frequency deletions detected in our work involved highly similar sequences separated by more than 150 base pairs.

The Hu19-CD828Z anti-CD19 CAR that is part of all bicistronic constructs developed during this project has already been proven effective in a clinical trial[10]; therefore, we focused further work on optimizing

the anti-CD20 scFv that was included in the second CAR of the constructs that we developed. We hypothesized that a longer glycine-serine linker in this scFv might affect function of the anti-CD20 CAR. One possible advantage of longer linkers is that scFvs have a decreased tendency to multimerize as linker length increases.[41] We compared an anti-CD19/CD20 bicistronic construct that included an anti-CD20 CAR scFv with a standard linker of three repeats of G-G-G-G-S (Hu1928-Hu20BB-STD) to a construct that was identical to STD, except the anti-CD20 CAR scFv had a linker of four repeats of G-G-G-G-S. This anti-CD19/CD20 construct with a longer anti-CD20 CAR scFv linker was designated LONG. T cells expressing LONG had functional benefits in CD20-specific function when compared with T cells expressing STD. T cells expressing LONG had higher levels of CD20-specific IL-2 release (Figure 4B), more retention of anti-CD20 CAR expression after stimulation with $CD20^+$ target cells (Figures 4E and 4F), and lower levels of AICD (Figures 4G and 4H). CAR T cells exhibit substantial levels of AICD in the assay that we used, but we have noted similar levels of AICD with other CARs.[27,42] Notably, the only advantage in antigen-specific IFN-γ release with LONG versus STD was that T cells expressing LONG had lower antigen-independent IFN-γ release against target cells lacking both CD19 and CD20 expression (Figure 4A). Similarly, we found no difference in antigen-specific degranulation when LONG and STD were compared (Figures 3J–M).

CAR expression assessed by MFI measured by flow cytometry was higher when Hu19-CD828Z or Hu20-CD8BBZ-L were expressed in separate T cells by vectors encoding each of these CARs individually versus when these CARs were expressed simultaneously in the same T cell by the bicistronic LONG construct (Figure S12). Despite the lower MFI for the CARs expressed by LONG versus CARs expressed one at a time, we did not see statistically significant differences in IFN-γ and IL-2 release with bicistronic CAR expression versus the same CARs expressed individually, and antigen-specific degranulation was statistically higher for T cells expressing LONG versus Hu20-CD8BBZ-L (Figures 6B, S11, S13, and S14).

Because T cells expressing LONG had *in vitro* functional advantages against $CD20^+$ target cells when compared with T cells expressing STD, we selected LONG for further development. T cells expressing LONG eliminated tumors of four different human tumor cell lines from NSG mice (Figures 5B–5E and 6C–6F). The main goal of this work was to develop a CAR T cell therapy that could eliminate CD19-negative tumors, and T cells expressing LONG were able to eliminate tumors of the CD19-negative cell lines CD20-MM.1S and st486-CD19neg (Figures 5D, 5E, and 6C–6D). Use of a bicistronic construct offers a clinical advantage of the potential to eradicate lymphoma cells lacking expression of either CD19 or CD20. With a bicistronic construct, both CD19 and CD20 can be targeted by T cells transduced with one vector. Using only one vector offers advantages of greater simplicity and lower expense when compared with a dual transduction strategy of transducing T cells with one vector encoding an anti-CD19 CAR and another vector encoding an anti-CD20 CAR. The production costs and regulatory requirements of producing one anti-CD19/CD20 bicistronic vector are the same as producing each of two vectors needed for a dual transduction strategy of one vector encoding an anti-CD19 CAR and another vector encoding an anti-CD20 CAR.

The design of LONG includes a CD28 costimulatory domain in the anti-CD19 CAR and a 4-1BB domain in the anti-CD20 CAR, so T cells encountering malignant cells expressing both CD19 and CD20 will receive costimulation from both CD28 and 4-1BB, the two costimulatory domains that are commonly used in CARs.[43] The extensive *in vitro* and *in vivo* testing of the LONG construct demonstrate the full range of T cell functions and efficient *in vivo* anti-tumor activity. We plan to test autologous T cells expressing the LONG construct in a clinical trial enrolling patients with B cell lymphoma. The clinical trial will enroll patients with lymphoma expressing CD19, CD20, or both CD19 and CD20.

METHODS

Human cells and mice

Peripheral blood mononuclear cells (PBMCs) from patients enrolled on National Cancer Institute (NCI) clinical trials were used. Use of patient samples for research was approved by the NCI Institutional Review Board. Informed consent was obtained from all patients. Animal studies were carried out on protocols approved by the NCI Animal Care and Use Committee.

Design and construction of plasmids encoding CARs

We previously designed the Hu19-CD828Z anti-CD19 CAR.[42] The scFv of this CAR was designated Hu19 and had the following DNA sequence from 5′ to 3′: human CD8α signal sequence (SS), a human light chain variable domain, a linker[44] (GSTSGSGKPGSGEGSTKG), and a human heavy chain variable domain. The Hu19-CD828Z-DNA sequence has the following components from 5′ to 3′: the Hu19 scFv, a hinge and transmembrane region from human CD8α (CD8-HTM), a CD28 costimulatory domain, and the CD3ζ T cell activation domain.

We incorporated Hu19-CD828Z into a bicistronic construct that also encoded a separate CAR targeting CD20. The first CAR in the construct was Hu19-CD828Z. Next was a F2A-containing ribosomal skip sequence.[45] F2A stands for the hand, foot, and mouth virus 2A sequence. After the F2A-containing sequence, came a furin cleavage site and then an anti-CD20 CAR. The anti-CD20 CAR was designated Hu20-CD8BBZ. The scFv of this CAR was designated Hu20 and had the following DNA sequence from 5′ to 3′: human CD8α SS, light chain variable domain, linker, and heavy chain variable domain. The Hu20 variable domains came from the human antibody 2.1.2. The variable domains were connected by a linker made up of three repeats of four glycines and one serine. The 2.1.2 antibody was derived by immunizing mice transgenic for human immunoglobulin genes.[46] After the Hu20 scFv, the Hu20-CD8BBZ CAR included these domains from 5′ to 3′: human CD8-HTM, human 4-1BB cytoplasmic region, and human CD3ζ T cell activation domain. The entire CAR construct including Hu19-CD828Z and Hu20-CD8BBZ with intervening F2A-containing sequence was designated Hu1928-Hu20BB-Original.

To prevent deletion events, we optimized the DNA sequence of Hu1928-Hu20BB-Original to eliminate repeated highly similar regions of DNA sequence. When repeated regions of highly similar DNA sequence were identified, we changed the sequence of DNA triplet codons by substituting an alternate DNA codon encoding the same amino acid. We used the GenScript Codon Usage Frequency Table (www.genscript.com/tools/codon-frequency-table) to select triplet codons commonly expressed in Homo sapiens. When we designed new sequences, DNA fragments were synthesized by Thermo/GeneArt with restriction sites at the 5′ and 3′ ends. We ligated these DNA fragments into restriction-enzyme-digested MSGV1 retroviral plasmids by using a Roche DNA ligation kit. In addition to these changes, we replaced the CD8α SS of the Hu20-CD8BBZ CAR with the SS of the GM-CSFr.[29] The optimal version of the sequence-optimized construct was designated Hu1928-Hu20BB-STD

We designed a construct designated LONG that has the same nucleotide sequence as STD except that the linker of the Hu20 scFv has been lengthened to include four repeats of four glycines and one serine (GGGGSGGGGSGGGGSGGGGS) instead of the three repeats of four glycine and one serine of the STD construct. The LONG plasmid was generated by replacing the sequence of the Hu20 scFv in STD with a newly synthesized DNA fragment (Thermo/GeneArt). We made a construct called Hu1928-Hu2028-Long that was identical to LONG, except that the 4-1BB domain of the anti-CD20 CAR was replaced with a CD28 domain.

We generated plasmids encoding each separate CAR of the LONG construct described above. These CARs, Hu19-CD828Z and Hu20-CD8BBZ-Long (Hu20-CD8BBZ-L), had the same optimized sequences included. MSGV1-SP6-CD828Z encodes a previously described negative control CAR.[29]

The sequences for CD8α, CD28, 4-1BB, and CD3ζ were from the National Center for Biotechnology Information website (www.ncbi.nlm.nih); sequences in CARs were based on prior work.[29]

Single molecule real-time RNA-seq analysis

SMRT RNA-seq was performed. RNA was extracted from unsorted cultures of CAR-transduced T cells for both SMRT and short-read RNA-seq experiments by using RNeasy Plus kits (Qiagen). Full-length cDNA was synthesized and amplified with the NEBNext Single Cell/Low Input cDNA Synthesis & Amplification Module (New England Biolabs) and the Iso-Seq Express Oligo Kit (PacBio). cDNA was amplified with 12 PCR cycles and size selected by using 0.84 × ProNex beads (Promega). SMRTbell libraries were then prepared with the SMRTbell Express Template Prep Kit 2.0 (PacBio). Transcripts above 2.5 kb were selected. Sequencing primer v4 was annealed to libraries. Sequel II polymerase 2.0 was bound to libraries, and the libraries were loaded on one SMRT Cell on the Sequel II System by using diffusion loading. Sequencing was performed with 2-h pre-extension and a 24-h movie.

Initial isoform predictions were created from long reads by using software from PacBio.[47] Processing of long reads was performed with SMRT Analysis Software from PacBio (www.pacb.com/products-and-services/analytical-software/smrt-analysis) by using computational resources of the National Institutes of Health High-performance Computing Biowulf cluster (http://hpc.nih.gov).

The reference sequence from hg38 was used. The program "ccs" was used to generate circular consensus sequences (ccs) from subreads. The program "lima" was then used to remove primers and demultiplex. The program "isoseq3 refine" was used to trim polyA tails and remove concatemers to produce full-length non-concatemer reads. The program "isoseq3 cluster" created putative isoforms. Next, the program "isoseq3 polish " was used to polish transcripts. The program "pbmm2 align," which uses minmap2,[48] was used to align reads to the reference and to create General Feature Format files. The program "isoseq3 collapse" was used to merge reads into isoforms.

Short-read RNA-seq analysis

Short-read RNA-seq (Illumina, Inc.), was performed. Library preparation was performed with an Illumina TruSeq stranded mRNA Library Prep. We used 1 μg total RNA as the input to an mRNA capture with oligo-dT-coated magnetic beads. The mRNA was fragmented, and then a random-primed cDNA synthesis was performed. Double-strand cDNA was synthesized and used as the input to a standard library preparation with adapter ligation with unique indexed barcodes. PCR amplification was performed to give a sequencing-ready library. The final purified product was quantitated by quantitative PCR before cluster generation and paired-end sequencing.

Analysis of short-read RNA-seq data in Table 2 and Figures S3–S8 was performed as follows. The fast-all (fasta) files for the CAR construct sequences were added to fasta files for the Genome Reference Consortium Human Build 38 (hg38)[49] including chromosomes 1 to 22 and chromosomes X, Y, and M (mitochondria). Reads were trimmed using Cutadapt version 1.18.[50]

Alignment was generated with STAR aligner version 2.7.8a[51] to create a binary alignment amp (bam) file and the "*sj.tab.output*" file that contains fields specifying the location of the intron and the number of uniquely mapping reads crossing the junction.

The coverage for each base in the CAR construct was obtained by using the command "depth command" option to samtools. This generated a count of coverage from all the aligned reads for each base of the construct. The count of coverage at the position of the splice acceptor was obtained; this number was referred to as "coverage at splice acceptor." This is a crude measure of the frequency of mature transcripts. The number of unique mapped reads for a deletion (splice) junction was used as a numerator and divided by this "coverage at splice acceptor" denominator to obtain a fraction. This approach is appropriate for comparing the relative frequencies of deletion (splice) junctions at different locations in the construct.

The genome index was created with the command "STAR genomeGenerate" by using parameter sjdbOverhang with a value of 100

and with Gencode.v35.annotation.gtf[52] and an additional section for the appropriate CAR construct.

Important parameters to star program were

–chimJunctionOverhangMin 12
12 –chimSegmentMin
–chimMultimapNmax 20
–alignSJDBoverhangMin 10
–alignMatesGapMax 100000
–alignIntronMax 100000
–alignSJstitchMismatchNmax 5-1 5 5
–chimMultimapScoreRange 3
–chimScoreJunctionNonGTAG −4
–chimNonchimScoreDropMin 10
–peOverlapNbasesMin 12
–peOverlapMMp 0.1
–outFilterMultimapNmax 20
–alignSJoverhangMin 8
–outFilterMismatchNmax 999
–outFilterMismatchNoverLmax 0.3
–alignIntronMin 20
–clip3pAdapterSeq -
–limitSjdbInsertNsj 4000000

The sj.tab.output file fields specifying the location of the intron and number of uniquely mapping reads crossing the junction were used for analysis.

The following methods were used only for the short-read RNA-seq analysis data in Table S1 and Figure S5. We assessed the sequencing quality of RNA-seq Fastq files (150 base pairs) with FastQC (https://www.bioinformatics.babraham.ac.uk/projects/fastqc), and we used BBDuk (https://sourceforge.net/projects/bbmap/) to trim the reads contaminated with Illumina adapters. We then aligned the trimmed reads to the CAR construct sequence by using the splicing-aware RNA-seq alignment tools STAR (version 2.7.3a) and HISAT2 (version 2.2.1).[51,53] To identify potential splicing sites, we applied R package SamSeq (https://github.com/jefferys/SamSeq) to remove unmapped, not primary alignment, failed vendor quality control reads, and reads not in a proper pair. We also removed soft-clipped aligned reads. Only reads with CIGAR string containing "N" (large gaps) or "D" (small deletion) tag and with at least a 3-bp gap length were retained for further analysis. For each variant candidate, we determined the consequences of the splicing event by translating the cDNA sequence to protein sequence using R package Seqinr, and we identified if it was a frameshift, stop codon, or point mutation.[54] We calculated an reads per kilobase per million mapped reads-like score to represent a standardized measurement of each potential splicing variant by using the number of aligned reads, and we used the sum of these scores for each variant and the normal sequence to estimate their mRNA percentages. Finally, we ranked the mRNA percentage in a decreasing manner and selected the top ranked variant candidates and corresponding bam files for visual validation in an Integrative Genomics Viewer.[55]

ddPCR

ddPCR was performed with a DNA concentration adjusted to result in no higher than 30% of wells yielding any CD8-HTM PCR product. The ddPCR was performed as described in Figure S6 with a BioRad ddPCR system and BioRad reagents. Sequences of primers in the ddPCR assay were:

Hu19 Fwd: GCACCCTGGTGACAGTG

CD28 Rev: GGTCATGTTCATGTAGTCGCT

4-1BB Fwd: CTATGGTGGCATGGATGTGT

4-1BB Rev2: ACAGCCATCTTCCTCTTGTG

CD8a hinge probe 6-carboxyfluorescein- CTACAATCG/ZEN/CCAGCCAGCCTCT-3 Iowa Black Fluoroquencher

Gamma-retroviral transductions and T cell culture

To produce replication-incompetent gamma-retroviruses, packaging cells were transfected with plasmids encoding CARs along with a plasmid encoding the RD114 envelope protein as previously described.[29] Human T cells were used in all experiments. Transduction of T cells with gamma-retroviruses encoding CAR constructs was performed as previously described 2 days after initiation of T cell cultures.[29] T cells were cultured as described previously.[29] In brief, PBMC were stimulated with the anti-CD3 monoclonal antibody OKT3 (OKT3, Orthoclone) in AIM V complete medium and 300 IU/mL IL-2 (Teceleukin, Roche). AIM V complete medium consisted of AIM V medium (Thermo), 5% human AB serum (Valley Biomedical), 100 U/mL penicillin, and 100 μg/mL streptomycin. Non-tissue-culture-treated six-well plates were coated with Retronectin (Takara). Two days after OKT3 stimulation, 2 mL gamma-retroviral supernatant was applied to each well of the retronectin-coated plates and incubated for 2 h at 37°C. Two milliliters of medium containing 2×10^6 cells were added directly to the viral supernatant. IL-2 was added at 300 IU/mL. Incubation was carried out at 37°C for 16–18 h. Next, cells were suspended in fresh medium plus IL-2. Cultures were maintained by suspending the cells at 0.5×10^6 cells/mL in AIM V complete media with 300 IU/mL IL-2 every 2 days.

Cell lines and primary cells

We previously transduced K562 cells to express CD19 (CD19-K562) or low-affinity nerve growth factor receptor (NGFR-K562).[29] We transduced both K562 cells and MM.1S cells (American Tissue Type Culture Collection [ATCC]) with a gamma-retroviral vector

encoding CD20 to generate CD20-K562 and CD20-MM.1S cells. NALM6 cells are $CD19^+$ and $CD20^+$ (acute lymphoid leukemia from DSMZ). St486 and Toledo were obtained from ATCC; both cell lines express CD20 and CD19. CD19 expression is weak on st486 cells. st486-CD19neg and Toledo-CD19neg had CD19 nearly eliminated by CRISPR/Cas9 in our laboratory; st486-CD19neg and Toledo-CD19neg expressed CD20. To generate st486-CD19neg and Toledo-CD19neg, lentiviral transduction was performed with two CD19-targeting single guide RNA molecules (GenScript, Broad Institute).

CD19 CRISPR guide RNA 1 = AAGCGGGGACTCCCGAGACC

CD19 CRISPR guide RNA 3 = TGGAATGTTTCGGACCTAGG

These cell lines lacking CD19 and CD20 expression were used: 293T (embryonic kidney), NGFR-K562 (myeloid leukemia), CCRF-CEM (T cell leukemia); A549 (lung carcinoma); TC71 (Ewings sarcoma, gift of M. Tsokos, NCI), COLO205 (colon carcinoma), U251 (glioblastoma), HEPG2 (hepatocellular carcinoma), and Panc10.05 (pancreatic carcinoma). These cell lines were from ATCC unless noted.

CAR detection on T cells and flow cytometry

Cell-surface CAR expression was detected with two non-commercial antibodies. The allophycocyanin (APC)-labeled anti-CD19-CAR antibody has been used in prior work and binds to the Hu19 scFv.[10] The pacific blue-labeled anti-CD20-CAR antibody binds to the Hu20 scFv. T cells (5×10^5) were suspended in 50 μL staining buffer (0.4% bovine serum albumin, 0.1% sodium azide in PBS), and antibodies were added. T cells were also stained with the following antibodies: CD3 APC-cyanine-7 clone UCHT1 (BD Biosciences); CD4 fluorescein isothiocyanate (FITC) clone RPA-T4 (BD Biosciences); CD8 R-phycoerythrin cyanine-7 (PE-Cy7/eFluor450) clone RPA-T8 (BD Biosciences or Thermo Scientific), C-C chemokine receptor 7 PE dazzle 594, clone G043H7 (Biolegend), and CD45RA FITC clone HI100 (Biolegend).

Flow cytometry was performed with a LSRFortessa (BD) or FACSymphony A5 (BD) cytometers. Dead cells were excluded with 7-amino-actinomycin D (7-aad; BD Biosciences). The gating strategy is shown in Figure S16. Flow cytometry analysis for all experiments was performed with FlowJo (Tree Star, Inc.).

CD107a assay

For each culture tested, tubes containing each target cell type were prepared. All tubes also contained CAR-transduced T cells, 1 mL AIM-V complete medium, R-PE-labeled anti-CD107a antibody (Clone H4A3; Thermo Scientific), and 1 μL Golgi Stop (monensin; BD). Tubes were incubated at 37°C for 4 h and then stained for CD3, CD4, and CD8. Samples were analyzed by flow cytometry. Normalization was conducted by dividing the percentage of $CD4^+$ or $CD8^+$ T cells that were $CD107a^+$ by the percentage of $CD4^+$ or $CD8^+$ T cells that were CAR^+.

Cytotoxicity assays

Cytotoxicity assays were conducted as previously described.[29,56] Cytotoxicity was measured by comparing survival of $CD19^+$, $CD20^+$ Toledo target cells relative to the survival of negative-control, CD19-negative, CD20-negative CCRF-CEM cells. Both cell types were combined in the same tubes with CAR-transduced T cells. CCRF-CEM cells were labeled with 5-(and-6)-(((4-chloromethyl)benzoyl)amino) tetramethylrhodamine (CMTMR; Thermo Scientific), and Toledo cells were labeled with carboxyfluorescein diacetate succinimidyl ester (CFSE; Thermo Scientific). In some experiments, CAR T cell cultures were depleted of natural killer cells with a Stem Cell Technologies CD56 positive-selection kit before use in cytotoxicity assays. Cultures were set up in sterile 5-mL test tubes (BD) in duplicate at multiple T cell to target cell ratios. The target cells contained in the tubes were 50,000 CFSE-labeled Toledo cells and 50,000 CMTMR-labeled CCRF-CEM cells. Cultures were incubated for 4 h at 37°C. Immediately after the incubation, 7-aad (BD Biosciences) was added, and flow cytometry acquisition was performed. For each T cell plus target cell culture, the percent survival of Toledo cells was determined by dividing the percent live Toledo cells by the percent live CCRF-CEM negative-control cells. The corrected percent survival of Toledo cells was calculated by dividing the percent survival of Toledo cells in each T cell plus target-cell culture by the ratio of the percent live Toledo cells to the percent live CCRF-CEM cells in tubes containing only Toledo cells and CCRF-CEM cells without effector T cells. This correction was necessary to account for variation in the starting cell numbers and for spontaneous target cell death. Cytotoxicity was calculated as follows: the percent cytotoxicity of Toledo cells = 100 – corrected percent survival of Toledo target cells.

Annexin V staining

CAR-transduced T cells were incubated for 4 h in 24-well plates with either st486-CD19neg, or NGFR-K562 target cells. There were 1.5×10^6 T-cells and 1×10^6 target cells in each well. After incubation, cells were stained with anti-CD19-CAR antibodies, anti-CD20-CAR antibodies, CD3, CD4, and CD8. Cells were washed twice with PBS, re-suspended in Annexin V Binding buffer (BD Biosciences), and incubated with APC-conjugated Annexin V (BD Biosciences) and 7-aad (BD Biosciences) for 15 min at room temperature. Cells were then immediately analyzed by flow cytometry.

ELISA

Target cells were combined with CAR-transduced T cells in duplicate wells of a 96-well round bottom plate at a 1:1 effector:target ratio. The cells were cultured in AIM-V medium+5% human serum at 37°C for 18–20 h. Following the incubation, ELISAs for IFN-γ were performed on the culture supernatant by using standard methods as previously described.[27] IL-2 ELISAs (R&D Systems) were performed as recommended by the manufacturer. When two or more CARs were compared, cytokine release was normalized for CAR expression by dividing cytokine levels by the fraction of CAR^+ T cells.

Proliferation assays

Cultures were set up in 24-well plates. Target cells included in cultures were either CD19-K562 or CD20-K562 or NGFR-K562. Target cells

were all irradiated, and 0.5×10^6 target cells were used. The cultures included 0.75×10^6 CAR T cells. The T cells were labeled with CFSE as previously described.[57] AIM V medium + 5% human serum without IL-2 was used. Four days after initiation, live cells in each culture were counted with trypan blue for dead cell exclusion. Flow cytometry was performed after staining with anti-CD19-CAR, anti-CD20-CAR, anti-CD3, anti-CD4, and anti-CD8. Antigen-specific proliferation was presented as CFSE MFI of T cells stimulated with either CD19-K562 or CD20-K562 divided by the CFSE MFI of T cells stimulated with NGFR-K562.

Murine experiments

Seven- to 9-week-old NOD.Cg-Prkdcscid Il2rgtm1Wjl/SzJ (NSG) mice from NCI-Frederick or Jackson Laboratories were used. Measurable tumors were present before CAR T cell injection in all experiments. For all tumor cell lines, 4×10^6 cells were injected intradermally in a 1:1 mix of Matrigel (Corning) and PBS 6–7 days before CAR T cell injection. CAR T cells from cultures initiated seven days before injection were injected intravenously at $CD3^+CAR^+$ cell doses indicated in figure legends. Mice received one CAR T cell injection. Tumors were measured using a caliper every 3 days. Volumes of tumors were calculated using the formula (length × width × height)/2. Mice were sacrificed once tumors reached 15 mm in longest length. Tumor volume curves ended when the first mouse of a group was sacrificed or the experiment ended.

Statistics

Statistics are described in figure legends and were performed with GraphPad Prism Version 8.4.3. A p value of <0.05 was considered statistically significant. All analyses were two tailed. Corrections for multiple comparisons were not performed.

DATA AND CODE AVAILABILITY

The authors will provide any primary data for results presented in this publication upon request. Upon reasonable request, we will provide materials not commercially available that were used in this work. GenBank accession codes of novel CARs reported in this manuscript are as follows in the format of CAR construct name, accession number: LONG, ON023113; Hu1928-Hu20BB-STD, ON023114; Hu1928-Hu2028-Long, ON023115; Hu19-CD828Z, ON023116; Hu20-CD8BBZ, ON023117; Hu20-CD8BBZ-Long, ON023118; Hu1928-Hu20BB-Original, ON023119.

SUPPLEMENTAL INFORMATION

Supplemental information can be found online at https://doi.org/10.1016/j.omto.2023.07.001.

ACKNOWLEDGMENTS

We thank the animal care staff of the National Institutes of Health (NIH) Clinical Research Center animal facility. We also thank the staff of the National Cancer Institute (NCI), Surgery Branch flow cytometry core facility. We thank Elizabeth Tseng (PacBio Technologies) for advice on SMRT analysis. Funding for this work was from NIH, NCI intramural funding, and from a research agreement between NCI and Kite, a Gilead Company. X.W. is supported by federal funds from the NIH and the NCI, under contract no. 75N91019D00024.

This work was supported in part by intramural funding of the Center for Cancer Research, National Cancer Institute, NIH. The content of this publication does not necessarily reflect the views or policies of the Department of Health and Human Services, nor does mention of trade names, commercial products, or organizations imply endorsement by the U.S. government.

AUTHOR CONTRIBUTIONS

N.L. conducted experiments, designed experiments, analyzed data, and wrote the manuscript. J.N.K. led the project, designed the CARs, analyzed data, and wrote the manuscript. S.Y., S.C., C.A., and L.C. conducted experiments and analyzed data. R.F. and M.C. conducted the analysis of the sequencing data. J.A. and L.H. performed bioinformatics analysis. X.W. designed and performed the ddPCR assay. All authors edited the manuscript.

DECLARATION OF INTERESTS

N.L. is an inventor on a patent application for CAR constructs reported in this manuscript. S.Y. is an inventor on a patent application for CAR constructs reported in this manuscript. J.K. is an inventor on patent applications for CAR constructs reported in this manuscript and is principal investigator of a research agreement that involves NCI receiving research funding from Kite, a Gilead Company. J.A. and L.H. are employees of Kite, a Gilead Company, and are inventors on a provisional patent application named "Bioinformatics methods for the detection and characterization of splicing events for CARs" reported in this manuscript (Table S1; and Figure S4). No other authors had competing financial interests.

REFERENCES

1. Dotti, G., Gottschalk, S., Savoldo, B., and Brenner, M.K. (2014). Design and development of therapies using chimeric antigen receptor-expressing T cells. Immunol. Rev. *257*, 107–126. https://doi.org/10.1111/imr.12131.

2. Jensen, M.C., and Riddell, S.R. (2015). Designing chimeric antigen receptors to effectively and safely target tumors. Curr. Opin. Immunol. *33*, 9–15. https://doi.org/10.1016/j.coi.2015.01.002.

3. Sadelain, M. (2015). CAR therapy: The CD19 paradigm. J. Clin. Invest. *125*, 3392–3400. https://doi.org/10.1172/JCI80010.

4. Eshhar, Z., Waks, T., Gross, G., and Schindler, D.G. (1993). Specific activation and targeting of cytotoxic lymphocytes through chimeric single chains consisting of antibody-binding domains and the gamma or zeta subunits of the immunoglobulin and T-cell receptors. Proc. Natl. Acad. Sci. USA *90*, 720–724.

5. Kochenderfer, J.N., Wilson, W.H., Janik, J.E., Dudley, M.E., Stetler-Stevenson, M., Feldman, S.A., Maric, I., Raffeld, M., Nathan, D.A.N., Lanier, B.J., et al. (2010). Eradication of B-lineage cells and regression of lymphoma in a patient treated with autologous T cells genetically engineered to recognize CD19. Blood *116*, 4099–4102.

6. Kochenderfer, J.N., Dudley, M.E., Kassim, S.H., Somerville, R.P.T., Carpenter, R.O., Stetler-Stevenson, M., Yang, J.C., Phan, G.Q., Hughes, M.S., Sherry, R.M., et al. (2015). Chemotherapy-refractory diffuse large B-cell lymphoma and indolent B-cell malignancies can be effectively treated with autologous T cells expressing an anti-CD19 chimeric antigen receptor. J. Clin. Oncol. *33*, 540–549. https://doi.org/10.1200/JCO.2014.56.2025.

7. Turtle, C.J., Hanafi, L.A., Berger, C., Gooley, T.A., Cherian, S., Hudecek, M., Sommermeyer, D., Melville, K., Pender, B., Budiarto, T.M., et al. (2016). CD19

CAR-T cells of defined CD4+:CD8+ composition in adult B cell ALL patients. J. Clin. Invest. *126*, 2123–2138. https://doi.org/10.1172/JCI85309.

8. Neelapu, S.S., Locke, F.L., Bartlett, N.L., Lekakis, L.J., Miklos, D.B., Jacobson, C.A., Braunschweig, I., Oluwole, O.O., Siddiqi, T., Lin, Y., et al. (2017). Axicabtagene ciloleucel CAR T-cell therapy in refractory large B-Cell lymphoma. N. Engl. J. Med. *377*, 2531–2544. https://doi.org/10.1056/NEJMoa1707447.

9. Schuster, S.J., Bishop, M.R., Tam, C.S., Waller, E.K., Borchmann, P., McGuirk, J.P., Jäger, U., Jaglowski, S., Andreadis, C., Westin, J.R., et al. (2019). Tisagenlecleucel in adult relapsed or refractory diffuse large B-cell lymphoma. N. Engl. J. Med. *380*, 45–56. https://doi.org/10.1056/NEJMoa1804980.

10. Brudno, J.N., Lam, N., Vanasse, D., Shen, Y.W., Rose, J.J., Rossi, J., Xue, A., Bot, A., Scholler, N., Mikkilineni, L., et al. (2020). Safety and feasibility of anti-CD19 CAR T cells with fully human binding domains in patients with B-cell lymphoma. Nat. Med. *26*, 270–280. https://doi.org/10.1038/s41591-019-0737-3.

11. Abramson, J.S., Palomba, M.L., Gordon, L.I., Lunning, M.A., Wang, M., Arnason, J., Mehta, A., Purev, E., Maloney, D.G., Andreadis, C., et al. (2020). Lisocabtagene maraleucel for patients with relapsed or refractory large B-cell lymphomas (TRANSCEND NHL 001): a multicentre seamless design study. The Lancet *396*, 839–852. https://doi.org/10.1016/S0140-6736(20)31366-0.

12. Kochenderfer, J.N., Somerville, R.P.T., Lu, T., Shi, V., Bot, A., Rossi, J., Xue, A., Goff, S.L., Yang, J.C., Sherry, R.M., et al. (2017). Lymphoma Remissions Caused by Anti-CD19 Chimeric Antigen Receptor T Cells Are Associated With High Serum Interleukin-15 Levels. J. Clin. Oncol. *35*, 1803–1813. https://doi.org/10.1200/jco.2016.71.3024.

13. Brudno, J.N., and Kochenderfer, J.N. (2018). Chimeric antigen receptor T-cell therapies for lymphoma. Nat. Rev. Clin. Oncol. *15*, 31–46. https://doi.org/10.1038/nrclinonc.2017.128.

14. Brudno, J.N., and Kochenderfer, J.N. (2016). Toxicities of chimeric antigen receptor T cells: recognition and management. Blood *127*, 3321–3330.

15. Kenderian, S.S., Porter, D.L., and Gill, S. (2017). Chimeric Antigen Receptor T Cells and Hematopoietic Cell Transplantation: How Not to Put the CART Before the Horse. Biol. Blood Marrow Transpl. *23*, 235–246. https://doi.org/10.1016/j.bbmt.2016.09.002.

16. Plaks, V., Rossi, J.M., Chou, J., Wang, L., Poddar, S., Han, G., Wang, Z., Kuang, S.Q., Chu, F., Davis, R.E., et al. (2021). CD19 target evasion as a mechanism of relapse in large B-cell lymphoma treated with axicabtagene ciloleucel. Blood *138*, 1081–1085. https://doi.org/10.1182/blood.2021010930.

17. Anderson, K.C., Bates, M.P., Slaughenhoupt, B.L., Pinkus, G.S., Schlossman, S.F., and Nadler, L.M. (1984). Expression of human B cell-associated antigens on leukemias and lymphomas: A model of human B cell differentiation. Blood *63*, 1424–1433. https://doi.org/10.1182/blood.v63.6.1424.1424.

18. Freedman, A. (2018). Follicular lymphoma: 2018 update on diagnosis and management. Am. J. Hematol. *93*, 296–305. https://doi.org/10.1002/ajh.24937.

19. Gökbuget, N., and Hoelzer, D. (2006). Novel antibody-based therapy for acute lymphoblastic leukaemia. Best Pract. Res. Clin. Haematol. *19*, 701–713. https://doi.org/10.1016/j.beha.2006.06.008.

20. Keating, M., and O'Brien, S. (2000). High-dose rituximab therapy in chronic lymphocytic leukemia. Semin. Oncol. *27*, 86–90.

21. Delviks-Frankenberry, K., Galli, A., Nikolaitchik, O., Mens, H., Pathak, V.K., and Hu, W.S. (2011). Mechanisms and factors that influence high frequency retroviral recombination. Viruses *3*, 1650–1680. https://doi.org/10.3390/v3091650.

22. Pathak, V.K., and Hu, W.S. (1997). "Might as well jump!' template switching by retroviral reverse transcriptase, defective genome formation, and recombination. Semin. Virol. *8*, 141–150. https://doi.org/10.1006/smvy.1997.0114.

23. Delviks, K.A., and Pathak, V.K. (1999). Effect of distance between homologous sequences and 3' homology on the frequency of retroviral reverse transcriptase template switching. J. Virol. *73*, 7923–7932. https://doi.org/10.1128/jvi.73.10.7923-7932.1999.

24. Hu, W.S., Bowman, E.H., Delviks, K.A., and Pathak, V.K. (1997). Homologous recombination occurs in a distinct retroviral subpopulation and exhibits high negative interference. J. Virol. *71*, 6028–6036. https://doi.org/10.1128/jvi.71.8.6028-6036.1997.

25. Pathak, V.K., and Temin, H.M. (1990). Broad spectrum of in vivo forward mutations, hypermutations, and mutational hotspots in a retroviral shuttle vector after a single replication cycle: Substitutions, frameshifts, and hypermutations. Proc. Natl. Acad. Sci. USA *87*, 6019–6023. https://doi.org/10.1073/pnas.87.16.6019.

26. Hughes, M.S., Yu, Y.Y.L., Dudley, M.E., Zheng, Z., Robbins, P.F., Li, Y., Wunderlich, J., Hawley, R.G., Moayeri, M., Rosenberg, S.A., and Morgan, R.A. (2005). Transfer of a TCR gene derived from a patient with a marked antitumor response conveys highly active T-cell effector functions. Hum. Gene Ther. *16*, 457–472.

27. Lam, N., Trinklein, N.D., Buelow, B., Patterson, G.H., Ojha, N., and Kochenderfer, J.N. (2020). Anti-BCMA chimeric antigen receptors with fully human heavy-chain-only antigen recognition domains. Nat. Commun. *11*, 283. https://doi.org/10.1038/s41467-019-14119-9.

28. Fang, G., Weiser, B., Visosky, A., Moran, T., and Burger, H. (1999). PCR-mediated recombination: A general method applied to construct chimeric infectious molecular clones of plasma-derived HIV-1 RNA. Nat. Med. *5*, 239–242. https://doi.org/10.1038/5607.

29. Kochenderfer, J.N., Feldman, S.A., Zhao, Y., Xu, H., Black, M.A., Morgan, R.A., Wilson, W.H., and Rosenberg, S.A. (2009). Construction and preclinical evaluation of an anti-CD19 chimeric antigen receptor. J. Immunother. *32*, 689–702.

30. Amatya, C., Pegues, M.A., Lam, N., Vanasse, D., Geldres, C., Choi, S., Hewitt, S.M., Feldman, S.A., and Kochenderfer, J.N. (2021). Development of CAR T Cells Expressing a Suicide Gene Plus a Chimeric Antigen Receptor Targeting Signaling Lymphocytic-Activation Molecule F7. Mol. Ther. *29*, 702–717. https://doi.org/10.1016/j.ymthe.2020.10.008.

31. Milone, M.C., Fish, J.D., Carpenito, C., Carroll, R.G., Binder, G.K., Teachey, D., Samanta, M., Lakhal, M., Gloss, B., Danet-Desnoyers, G., et al. (2009). Chimeric receptors containing CD137 signal transduction domains mediate enhanced survival of T cells and increased antileukemic efficacy in vivo. Mol. Ther. *17*, 1453–1464.

32. Wang, M., Munoz, J., Goy, A., Locke, F.L., Jacobson, C.A., Hill, B.T., Timmerman, J.M., Holmes, H., Jaglowski, S., Flinn, I.W., et al. (2020). KTE-X19 CAR T-Cell Therapy in Relapsed or Refractory Mantle-Cell Lymphoma. N. Engl. J. Med. *382*, 1331–1342. https://doi.org/10.1056/NEJMoa1914347.

33. Olejniczak, S.H., Stewart, C.C., Donohue, K., and Czuczman, M.S. (2006). A quantitative exploration of surface antigen expression in common B-cell malignancies using flow cytometry. Immunol. Invest. *35*, 93–114. https://doi.org/10.1080/08820130500496878.

34. Ladetto, M., Bergui, L., Ricca, I., Campana, S., Pileri, A., and Tarella, C. (2000). Rituximab anti-CD20 monoclonal antibody induces marked but transient reductions of peripheral blood lymphocytes in chronic lymphocytic leukaemia patients. Med. Oncol. *17*, 203–210. https://doi.org/10.1007/BF02780529.

35. Mikkilineni, L., and Kochenderfer, J.N. (2021). CAR T cell therapies for patients with multiple myeloma. Nat. Rev. Clin. Oncol. *18*, 71–84. https://doi.org/10.1038/s41571-020-0427-6.

36. Shah, N.N., Johnson, B.D., Schneider, D., Zhu, F., Szabo, A., Keever-Taylor, C.A., Krueger, W., Worden, A.A., Kadan, M.J., Yim, S., et al. (2020). Bispecific anti-CD20, anti-CD19 CAR T cells for relapsed B cell malignancies: a phase 1 dose escalation and expansion trial. Nat. Med. *26*, 1569–1575. https://doi.org/10.1038/s41591-020-1081-3.

37. Spiegel, J.Y., Patel, S., Muffly, L., Hossain, N.M., Oak, J., Baird, J.H., Frank, M.J., Shiraz, P., Sahaf, B., Craig, J., et al. (2021). CAR T cells with dual targeting of CD19 and CD22 in adult patients with recurrent or refractory B cell malignancies: a phase 1 trial. Nat. Med. *27*, 1419–1431. https://doi.org/10.1038/s41591-021-01436-0.

38. Tang, Y., Yin, H., Zhao, X., Jin, D., Liang, Y., Xiong, T., Li, L., Tang, W., Zhang, J., Liu, M., et al. (2022). High efficacy and safety of CD38 and BCMA bispecific CAR-T in relapsed or refractory multiple myeloma. J. Exp. Clin. Cancer Res. *41*, 2. https://doi.org/10.1186/s13046-021-02214-z.

39. Wang, X., Dong, Z., Awuah, D., Chang, W.C., Cheng, W.A., Vyas, V., Cha, S.C., Anderson, A.J., Zhang, T., Wang, Z., et al. (2022). CD19/BAFF-R dual-targeted CAR T cells for the treatment of mixed antigen-negative variants of acute lymphoblastic leukemia. Leukemia *36*, 1015–1024. https://doi.org/10.1038/s41375-021-01477-x.

40. Wang, Y., Zhong, K., Ke, J., Chen, X., Chen, Y., Shu, W., Chen, C., Hu, S., Sun, X., Huang, H., et al. (2021). Combined 4-1BB and ICOS co-stimulation improves anti-tumor efficacy and persistence of dual anti-CD19/CD20 chimeric antigen receptor T cells. Cytotherapy *23*, 715–723. https://doi.org/10.1016/j.jcyt.2021.02.117.

41. Desplancq, D., King, D.J., Lawson, A.D., and Mountain, A. (1994). Multimerization behaviour of single chain fv variants for the tumour-binding antibody b72.3. Protein Eng. *7*, 1027–1033. https://doi.org/10.1093/protein/7.8.1027.

42. Alabanza, L., Pegues, M., Geldres, C., Shi, V., Wiltzius, J.J.W., Sievers, S.A., Yang, S., and Kochenderfer, J.N. (2017). Function of Novel Anti-CD19 Chimeric Antigen Receptors with Human Variable Regions Is Affected by Hinge and Transmembrane Domains. Mol. Ther. *25*, 2452–2465. https://doi.org/10.1016/j.ymthe.2017.07.013.

43. Cappell, K.M., and Kochenderfer, J.N. (2021). A comparison of chimeric antigen receptors containing CD28 versus 4-1BB costimulatory domains. Nat. Rev. Clin. Oncol. *18*, 715–727. https://doi.org/10.1038/s41571-021-00530-z.

44. Whitlow, M., Bell, B.A., Feng, S.L., Filpula, D., Hardman, K.D., Hubert, S.L., Rollence, M.L., Wood, J.F., Schott, M.E., Milenic, D.E., et al. (1993). An improved linker for single-chain fv with reduced aggregation and enhanced proteolytic stability. Protein Eng. *6*, 989–995. https://doi.org/10.1093/protein/6.8.989.

45. Yang, S., Cohen, C.J., Peng, P.D., Zhao, Y., Cassard, L., Yu, Z., Zheng, Z., Jones, S., Restifo, N.P., Rosenberg, S.A., and Morgan, R.A. (2008). Development of optimal bicistronic lentiviral vectors facilitates high-level TCR gene expression and robust tumor cell recognition. Gene Ther. *15*, 1411–1423. https://doi.org/10.1038/gt.2008.90.

46. Gazit-Born-Stein, G., Green, L.L., Yang, X., Queva, C., and Blakey, D.C. (2006). Antibodies Directed to CD20 and Uses Thereof. Patent Application International Publication Number WO 2006/130458 A2.

47. Eid, J., Fehr, A., Gray, J., Luong, K., Lyle, J., Otto, G., Peluso, P., Rank, D., Baybayan, P., Bettman, B., et al. (2009). Real-time DNA sequencing from single polymerase molecules. Science *323*, 133–138. https://doi.org/10.1126/science.1162986.

48. Li, H. (2018). Minimap2: Pairwise alignment for nucleotide sequences. Bioinformatics *34*, 3094–3100. https://doi.org/10.1093/bioinformatics/bty191.

49. Schneider, V.A., Graves-Lindsay, T., Howe, K., Bouk, N., Chen, H.C., Kitts, P.A., Murphy, T.D., Pruitt, K.D., Thibaud-Nissen, F., Albracht, D., et al. (2017). Evaluation of GRCh38 and de novo haploid genome assemblies demonstrates the enduring quality of the reference assembly. Genome Res. *27*, 849–864. https://doi.org/10.1101/gr.213611.116.

50. Martin, M. (2011). Cutadapt removes adapter sequences from high-throughputsequencing reads. Embnet. J. *17*, 10–12.

51. Dobin, A., Davis, C.A., Schlesinger, F., Drenkow, J., Zaleski, C., Jha, S., Batut, P., Chaisson, M., and Gingeras, T.R. (2013). STAR: Ultrafast universal RNA-seq aligner. Bioinformatics *29*, 15–21. https://doi.org/10.1093/bioinformatics/bts635.

52. Frankish, A., Diekhans, M., Ferreira, A.M., Johnson, R., Jungreis, I., Loveland, J., Mudge, J.M., Sisu, C., Wright, J., Armstrong, J., et al. (2019). GENCODE reference annotation for the human and mouse genomes. Nucleic Acids Res. *47*, D766–D773. https://doi.org/10.1093/nar/gky955.

53. Kim, D., Langmead, B., and Salzberg, S.L. (2015). HISAT: A fast spliced aligner with low memory requirements. Nat. Methods *12*, 357–360. https://doi.org/10.1038/nmeth.3317.

54. Charif, D.L.J. (2007). SeqinR 1.0-2: a contributed package to the R project for statistical computing devoted to biological sequences retrieval and analysis. In Structural Approaches to Sequence Evolution: Molecules, Networks, Populations, P.M. Bastolla U, H. Roman, and M. Vendruscolo, eds.

55. Robinson, J.T., Thorvaldsdóttir, H., Winckler, W., Guttman, M., Lander, E.S., Getz, G., and Mesirov, J.P. (2011). Integrative genomics viewer. Nat. Biotechnol. *29*, 24–26. https://doi.org/10.1038/nbt.1754.

56. Hermans, I.F., Silk, J.D., Yang, J., Palmowski, M.J., Gileadi, U., McCarthy, C., Salio, M., Ronchese, F., and Cerundolo, V. (2004). The VITAL assay: a versatile fluorometric technique for assessing CTL- and NKT-mediated cytotoxicity against multiple targets in vitro and in vivo. J. Immunol. Methods *285*, 25–40.

57. Mannering, S.I., Morris, J.S., Jensen, K.P., Purcell, A.W., Honeyman, M.C., Van Endert, P.M., and Harrison, L.C. (2003). A sensitive method for detecting proliferation of rare autoantigen- specific human T cells. J. Immunol. Methods *283*, 173–183.